

Hierarchical Features Matter: A Deep Exploration of Progressive Parameterization Method for Dataset Distillation

Xinhao Zhong^{1,*} Hao Fang^{3,*} Bin Chen^{1,2†} Xulin Gu¹ Meikang Qiu⁴ Shuhan Qi¹ Shu-Tao Xia^{2,3}

¹Harbin Institute of Technology, Shenzhen ²Peng Cheng Laboratory

³Tsinghua Shenzhen International Graduate School, Tsinghua University ⁴Augusta University

xh021213@gmail.com, fang-h23@mails.tsinghua.edu.cn, chenbin2021@hit.edu.cn, 210110720@stu.hit.edu.cn, shuhanqi@cs.hitsz.edu.cn, qiumeikang@yahoo.com, xiast@sz.tsinghua.edu.cn;

Abstract

Dataset distillation is an emerging dataset reduction method, which condenses large-scale datasets while maintaining task accuracy. Current parameterization methods achieve enhanced performance under extremely high compression ratio by optimizing determined synthetic dataset in informative feature domain. However, they limit themselves to a fixed optimization space for distillation, neglecting the diverse guidance across different informative latent spaces. To overcome this limitation, we propose a novel parameterization method dubbed Hierarchical Parameterization Distillation (H-PD), to systematically explore hierarchical feature within provided feature space (e.g., layers within pre-trained generative adversarial networks). We verify the correctness of our insights by applying the hierarchical optimization strategy on GAN-based parameterization method. In addition, we introduce a novel class-relevant feature distance metric to alleviate the computational burden associated with synthetic dataset evaluation, bridging the gap between synthetic and original datasets. Experimental results demonstrate that the proposed H-PD achieves a significant performance improvement under various settings with equivalent time consumption, and even surpasses current generative distillation using diffusion models under extreme compression ratios $IPC=1$ and $IPC=10$. Our code is available at <https://github.com/ndhg1213/H-PD>

1. Introduction

In recent years, deep learning has made significant strides in various research fields, encompassing computer vision [13, 19] and natural language processing [3, 12]. These advancements have been facilitated by utilizing larger and more intricate deep neural networks (DNNs) in conjunction with

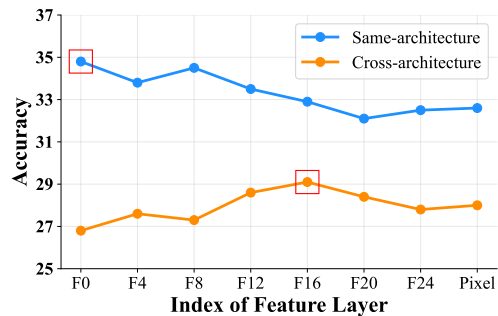


Figure 1. Performance of synthetic datasets condensed from various feature domains provided by GAN under the same settings (DSA on ImageNet-Birds).

numerous datasets tailored for diverse application fields. However, as the complexity of various learning tasks increases, neural networks have grown both deeper and wider, resulting in an exponential surge in the size of datasets required for training these models. This has presented a substantial challenge to data storage and processing efficiency [26], further exacerbating the bottleneck in deep learning due to the mismatch between the enormous data volume and limited computing resources.

Dataset distillation (DD) [44] has emerged as a promising solution to the aforementioned issues. It allows for the generation of a more compact synthetic dataset, where each data point encapsulates a higher concentration of task-specific information than its real counterparts. When trained on the synthetic dataset, the network can achieve performance comparable to its counterpart using the original dataset. By significantly reducing the size of the training data, dataset distillation offers a substantial reduction in training costs and memory consumption. Various methods have been proposed to enhance the performance of the condensed dataset.

Subsequently, synthetic dataset parameterization methods [5, 27, 38, 49] employ differentiable operations to pro-

*Equal Contribution.

†Corresponding Author.

cess synthetic images, shifting the optimization space from pixels to feature domains. These methods benefit from the efficient guidance of hidden features, thus achieving better performance. However, existing parameterization methods focus on one fixed optimization space, overlooking the informative guidance across multiple corresponding feature domains. For example, FreD [38] optimizes the synthetic dataset in the low-frequency space using discrete cosine transform (DCT), while ignoring informative guidance in the high-frequency domain. In recent years, several recent studies have exploited the rich semantic information encoded in the generators to enhance dataset distillation. With the rapid advancement achieved by generative models, one category of distillation methods utilizes diffusion models [34] to generative informative samples [18, 40]. However, under high compression rates (i.e., IPC=1/10), these methods can degrade into coreset selection methods. Another category of distillation methods employs GANs in an optimization-based manner [5, 49] to parameterize the synthetic datasets and achieve reliable results.

In contrast to the aforementioned methods, GAN-based parameterization distillation methods possess an optimization space with richer semantic information. ITGAN[49] directly optimizes the initial latent space of GAN and achieves significant performance improvements on low-resolution datasets. To fully utilize the GAN prior, GLaD [5] decomposes the GAN structure and manually selects the intermediate layer, greatly enhancing the cross-architecture performance of the synthetic dataset. However, existing method exhibit a performance decrease in the same-architecture settings when coupled with certain dataset distillation methods as suggested in Figure 1. In this manner, even though synthetic datasets are condensed from the optimally selected intermediate layer through preliminary experiments by manual picking, the diverse model architectures still lead to changes in the optimal performance. As aforementioned parameterization methods, current GAN-based approaches limit the optimization space to a specific feature domain and necessitate extensive computing time and resources to manually select the optimal feature domain for different settings. This naturally raises a question: *Does a fixed optimization space meet the demands of dynamic data distribution and model architectures during parameterization dataset distillation?*

To address this question, we propose a straightforward and efficient approach based on the parameterization prior, Hierarchical Parameterization Distillation (H-PD), which explores the significance of hierarchical features. To verify our intuition, we design a well-design framework on GAN-based parameterization method. The proposed H-PD embraces adaptive exploration across all hierarchical feature domains within GAN models. Specifically, we decompose the GAN structure, undertaking a greedy search that spans

different hierarchical feature domains. During the distillation process, we optimize these hierarchical latents within the GAN model, guided by the loss from the dataset distillation task. Throughout this optimization, we track the best hierarchical latents at the current layer, feeding them into the next layer. This iterative process continues until the optimizer traverses the hierarchical layers and reaches the pixel domain. To mitigate the time-consuming nature of performance evaluation, we introduce a class-relevant feature distance metric between the synthetic and real datasets to search for the optimal latent feature. This metric serves as a performance estimation for the synthetic datasets, encapsulating the significance of hierarchical features. Crucially, our method explores hierarchical features more comprehensively than previous approaches, which only rely on a single fixed feature domain as image priors.

Our main contributions can be summarized as follows:

- We revisited the shortcomings of existing parameterization methods, and provided a novel parametrization framework to enhance their efficiency by leveraging information across various feature domains.
- Through a well-designed framework, we effectively enhanced the performance of GAN-based parameterization methods, demonstrating the validity of our insights.
- To mitigate the computational demands associated with searching feature domains, we introduce a novel class-relevant feature distance metric, saving valuable computational time by approximating the real performance of the synthetic dataset.

2. Related Work

2.1. Dataset Distillation

Dataset distillation was initially regarded as a meta-learning problem [44]. It involves minimizing the loss function of the synthetic dataset using a model trained on the synthetic dataset. Since then, several approaches have been proposed to enhance the performance of dataset distillation. One category of methods utilizes ridge regression models to approximate the inner loop optimization [1, 31, 32, 54]. Another category of methods selects an informative space as a proxy target to address the unrolled optimization problem. DC [51], DSA [48] and DCC [25] match the weight gradients of models trained on the real and synthetic dataset, while DM [50], CAFE [43] and DataDAM [35] use feature distance between the real and synthetic dataset as matching targets. MTT [4] and TESLA [10] match the model parameter trajectories obtained from training on the real dataset and the synthetic dataset. In recent years, some studies have argued that the bi-level optimization structure required by traditional dataset distillation is redundant and computationally expensive.

Other studies suggest that the pixel domain, where im-

ages reside, is considered a high-dimensional space. Therefore, performance improvement can be achieved by parameterizing the synthetic dataset and transferring the optimization space. IDC [21] and HaBa [27] perform optimization in a low-dimensional space using differentiable operations, while GLaD [5] and ITGAN [49] utilize the feature domain provided by GANs as the optimization space, both of them employ pre-trained GANs as priors. FreD [38] employs traditional compression methods (e.g., DCT) to provide a low-frequency space as the optimization space. However, existing parameterization methods fix the optimization space thus neglecting the guidance from multi-feature domains.

The proposed H-PD introduces an innovative approach to parameterizing synthetic datasets and be verified on GAN-based parameterization methods, representing a broader and more encompassing enhancement compared to previous approaches utilizing fixed optimization space.

2.2. GAN for parameterization distillation

GAN [8] is a deep generative model trained adversarially to learn the distribution of real images. Recent studies have shown that GANs can tackle inverse problems by mapping images into their latent space [6, 14–16, 33, 45], enabling tasks like image editing [2, 41]. Incorporating image distribution information into GAN enhances the performance of dataset distillation by utilizing GAN to parameterize the synthetic dataset. GLaD employs GAN (e.g., StyleGAN-XL [36]) as a prior and significantly improves the cross-architecture performance of the synthetic dataset by selecting the feature domain of GAN’s intermediate layers as the optimization space. However, it overlooks the fact that the optimal optimization space may vary when dealing with different datasets, even with the same dataset distillation method. Additionally, it ignores the guidance offered by GAN’s earlier layers.

Compared with the current dataset distillation methods [18, 40] based on diffusion models, which could be more suitable for generative methods. GLaD can achieve significantly better performance under extreme compression ratios of IPC=1 and IPC=10 by enhancing the optimization-based methods as an efficient plugin. With the observation, the proposed H-PD further explores hierarchical feature domains of pre-trained GANs to address the limitation of GLaD, resulting in a novel parameterization method that successfully leveraging informative guidance within unfixed optimization space.

3. Method

In this section, we first present the problem definition of dataset distillation and discuss existing methods that parameterize synthetic datasets using GANs. Subsequently, we delve into the specifics of our method, aiming to improve upon previous works by exploring the feature do-

main provided by GANs. Finally, we propose an alternative evaluation scheme that assesses the synthetic dataset’s performance by measuring the layer-wise feature distance between it and the real one.

3.1. Preliminaries

Dataset distillation necessitates a real large-scale dataset $\mathcal{T} = \{(\mathbf{x}_t^i, y_t^i)\}_{i=1}^{\mathcal{T}}$ and aims to create a smaller synthetic dataset $\mathcal{S} = \{(\mathbf{x}_s^i, y_s^i)\}_{i=1}^{\mathcal{S}}$ ($|\mathcal{S}| \ll |\mathcal{T}|$), minimizing the performance gap between models trained on the two datasets. To achieve this, a well-designed matching objective $\phi(\cdot)$ is employed to extract feature distances in a specific informative space, representing the performance gap between the real and synthetic datasets. The optimization process involves initializing the synthetic dataset from the real dataset and iteratively updating it by minimizing the feature distance, which can be formulated below:

$$S^* = \arg \min_{\mathcal{S}} \mathcal{M}(\phi(\mathcal{S}), \phi(\mathcal{T})), \quad (1)$$

where $\mathcal{M}(\cdot, \cdot)$ denotes some matching metric, e.g., neural network gradients [51], exacted features[50], and training trajectories[4].

Building upon these findings, methods that parameterize synthetic datasets shift the optimization space from the pixel domain to the feature domain by employing differentiable operations. For instance, GAN priors-based methods [5, 49] can be formulated uniformly below:

$$\mathbf{z}^* = \arg \min_{\mathbf{z} \in \mathcal{Z}} \mathcal{M}(\phi(G_w(\mathbf{z})), \phi(\mathcal{T})), \quad (2)$$

where $\mathbf{z} \in \mathcal{Z}$ represents the latent in a specific feature domain of a pre-trained generative model $G_w(\cdot)$. Guided by GAN priors, these methods demonstrate substantial performance improvements.

3.2. Theoretical Insights of Unfixed Optimization Space and Fixed Optimization Space

Previous parameterization methods distill knowledge within a fixed optimization space, where the starting point in a given feature domain is typically randomly initialized. In contrast, our proposed H-PD framework performs progressive optimization on the latents. Figure 2 provides a detailed comparison of the optimization processes in fixed versus flexible feature spaces. Beyond the limited guidance across various feature domains, the fixed optimization space encounters a critical bottleneck: it restricts further enhancement by limiting the selection of superior synthetic datasets based on explicit or implicit criteria. In particular, the optimization within a fixed space can be viewed as a continuous process. If a temporarily optimal result, denoted as S^i , is chosen before convergence, and the corresponding optimization epoch does not mark the end of the optimization trajectory, a fundamental issue arises: *should S^i serve*

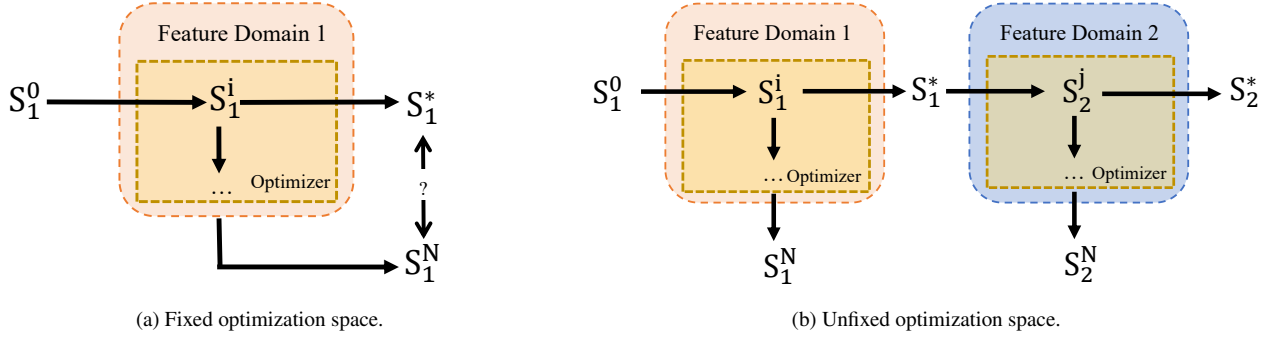


Figure 2. The comparison between fixed optimization space and unfixed optimization space. S^i is the synthetic dataset at optimization steps i , S^* is the optimal synthetic dataset selected during the optimization path, S_j is the synthetic dataset optimized in feature domain j .

as the starting point for the next phase of the optimization, or should the suboptimal result S^N be used instead? Opting for the latter can trap the optimization in a local minimum due to the absence of robust criterion-driven guidance, while choosing the former risks creating an optimization loop, effectively discarding the progress between S^i and S^N and forcing a reset.

Next, we provide the theoretical insights of its effectiveness. Specifically, we denote the random latent and optimized latent as \mathbf{z}_{rand} and \mathbf{z}_{opt} , respectively. For an effective dataset distillation method, we assume that the distilled data distribution $P(Z_{\text{lic}})$ fits the original dataset distribution in a lossless manner. Let the coupling latent $(\mathbf{z}_{\text{rand}}, \mathbf{z}_{\text{opt}})$ be the observed values of random variables Z_{rand} and Z_{opt} respectively. Let $c(\cdot)$ be a cost function defined in optimal transport theory [28], which satisfies $\mathbb{E}[c(X-Y)] \propto 1/I(X; Y)$. Then we can obtain:

$$\begin{aligned}
 & \mathbb{E}[c(Z_{\text{lic}} - Z_{\text{opt}})] \\
 = & k/D_{\text{KL}}(P(Z_{\text{lic}}, Z_{\text{opt}}) || P(Z_{\text{lic}}) \cdot P(Z_{\text{opt}})) \\
 = & k/[H(Z_{\text{lic}}) - H(Z_{\text{lic}}|Z_{\text{opt}})] \\
 \leq & k/[H(Z_{\text{lic}}) - H(Z_{\text{lic}}|Z_{\text{rand}})] \quad (3) \\
 = & k/D_{\text{KL}}(P(Z_{\text{lic}}, Z_{\text{rand}}) || P(Z_{\text{lic}}) \cdot P(Z_{\text{rand}})) \\
 = & \mathbb{E}[c(Z_{\text{lic}} - Z_{\text{rand}})],
 \end{aligned}$$

where k denotes a constant, $D_{\text{KL}}(\cdot||\cdot)$ and $H(\cdot)$ stand for Kullback-Leibler divergence and entropy, respectively. The Inequality (3) follows since the conditional entropy $H(Z_{\text{lic}}|Z_{\text{opt}})$ is smaller than $H(Z_{\text{lic}}|Z_{\text{rand}})$.

The theoretical analysis indicates that the proposed H-PD method of selecting partially optimized latents, rather than random initialization, reduces optimization cost across different spaces. By leveraging multiple feature domains, it accelerates convergence and, with its implicit evaluation criterion, effectively avoids local optima—an issue common in fixed optimization spaces.

3.3. Progressive Optimization with Hierarchical Feature Domains

To verify our insights about the utilization of unfixed parameterization optimization space, we apply it with GAN-based parameterization method (i.e., GLaD [5]). As depicted in Algorithm 1, our approach diverges from restricting the optimization space to a specific feature domain of the GANs. Instead, we aim to explore the hierarchical layers of the GAN, striving to enhance the effective utilization of the prior information.

To sufficiently utilize the informative guidance from the hierarchical feature domains, we decompose a pre-trained GAN $G_w(\cdot)$ for hierarchical layer searching, i.e.,

$$G_w(\cdot) = G_{K-1} \circ G_{K-2} \circ \dots \circ G_1 \circ G_0(\cdot). \quad (4)$$

For each hierarchical layer G_i provided by GAN, we repeat the following steps. Firstly, we generate images from \mathbf{z}_i only using the remaining synthesizing network $G_{k-1}(\cdot) \circ G_{k-2}(\cdot) \circ \dots \circ G_i(\cdot)$. Then, we employ the distillation method (e.g., MTT [4]) to calculate \mathcal{L} based on the synthetic dataset composed of generated images and the real dataset to optimize \mathbf{z}_i with an SGD optimizer, the optimization process lasts for a pre-determined and fixed N steps. After completing the optimization process for a specific layer, we implicitly evaluate the latents synthesized during the SGD optimization process and record \mathbf{z}_i^* as the optimal latents for the current layer. Finally, we pass \mathbf{z}_i^* into the next layer to obtain \mathbf{z}_{i+1}^0 as the initial latent for the next layer.

When the optimization space reaches the ultimate pixel domain, we choose the optimal latent \mathbf{z}^* from the recorded latents \mathbf{z}_i^* based on the real performance of the synthetic dataset \mathcal{S} generated by the corresponding remaining synthesizing network $G_{k-1}(\cdot) \circ G_{k-2}(\cdot) \circ \dots \circ G_i(\cdot)$. In this way, we fully explore the feature domain of the GAN, leveraging its rich information.

Algorithm 1 Pseudocode of H-PD with GAN-based parameterization method

Input: $G_w(\cdot)$: a pre-trained generative model; K : the number of hierarchical layers; N : distillation steps; \mathcal{T} : real training dataset; P_z : distribution of latent initializations; \mathcal{L} : distillation loss; $Acc(\cdot)$: evaluate real performance of synthetic dataset;

```
1: Initial average latent  $\mathbf{z} \sim P_z$ 
2: Dissemble  $G_w(\cdot)$  into  $G_{k-1} \circ G_{k-2} \circ \dots \circ G_0(\cdot)$ 
3:  $acc_{max} = 0$ 
4: for  $i \leftarrow 0$  to  $K - 1$  do
5:    $d_{min} = \mathcal{D}(G_{k-1} \circ \dots \circ G_i(\mathbf{z}_i^0), \mathcal{T})$ 
6:   for  $j \leftarrow 0$  to  $N - 1$  do
7:      $\mathcal{S}_i^j = G_{k-1} \circ \dots \circ G_i(\mathbf{z}_i^j)$ .
8:      $\mathcal{L} = \mathcal{M}(\phi(\mathcal{S}_i^j), \phi(\mathcal{T}))$ 
9:      $\mathbf{z}_i^{j+1} \leftarrow SGD(\mathbf{z}_i^j; \mathcal{L})$ 
10:    if  $\mathcal{D}(\mathcal{S}_i^j, \mathcal{T}) \leq d_{min}$  then
11:       $\mathbf{z}_i^* = \mathbf{z}_i^j, \mathcal{S}_i^* = \mathcal{S}_i^j$ 
12:    end if
13:  end for
14:  if  $Acc(\mathcal{S}_i^*) > acc_{max}$  then
15:     $acc_{max} = Acc(\mathcal{S}_i^*)$ 
16:     $\mathcal{S} = \mathcal{S}_i^*$ 
17:  end if
18:   $\mathbf{z}_{i+1}^0 = G_i(\mathbf{z}_i^*)$ 
19: end for
```

Output: Synthetic dataset \mathcal{S}

3.4. Enhancing Performance with Efficient Searching Strategy

Ensemble-Averaging Latent Initialization To mitigate the undesirable time overhead brought by existing methods [29] using clustering or GAN inversion [45], we propose an inactive searching initialization by calculating the average value of multiple noises, and passing it through the GAN’s mapping network to obtain the initial latent \mathbf{z}_0 with reduced bias. our method showcases simplicity without compromising effectiveness, as confirmed by sufficient experimental results.

Class-relevant Feature Distance To search for optimal latent as the optimization starting point of the subsequent feature domain, an efficient implicit evaluation metric is needed to replace the time-consuming evaluation of the synthetic dataset’s real performance. We first attempt to use the loss value as a substitute evaluation metric. However, it fails to yield desired results and, in some cases, performs even worse than not searching at all.

To utilize gradient information while maintaining diversity, we adopt the class activation map (CAM) [30] by utilizing the gradients of the corresponding class with respect

to the feature maps to localize the class-specific features. With the output logits $q = f^d(w^d; \mathbf{z})$ from the classifier w^d , the CAM is defined as the gradients of output logits q^y of class y with respect to features \mathbf{z} as follows:

$$g_{\mathbf{z}} = \frac{\partial q^y}{\partial \mathbf{z}}. \quad (5)$$

To focus attention on the class-relevant region, we propose a novel class-relevant feature distance $\mathcal{D}(\mathcal{S}, \mathcal{T})$ between the real dataset \mathcal{S} and the synthetic dataset \mathcal{T} . i.e.,

$$\mathcal{D}(\mathcal{S}, \mathcal{T}) = \left\| \frac{1}{|\mathcal{T}|} \sum_{i=1}^{|\mathcal{T}|} w^e(\mathbf{x}_t^i) \cdot \text{ReLU}(g_{\mathbf{z}}^t) - \frac{1}{|\mathcal{S}|} \sum_{j=1}^{|\mathcal{S}|} w^e(\mathbf{x}_s^j) \cdot \text{ReLU}(g_{\mathbf{z}}^s) \right\|^2, \quad (6)$$

where $w^e(\cdot)$ represents the feature extractor of a pre-trained network, and $\text{ReLU}(\cdot)$ is the rectified linear unit function.

4. Experiments

To verify the efficiency of our proposed method, we conduct experiments using code derived from the open-source GLaD¹. We utilize ImageNet-1K [11] subsets and CIFAR-10 [22] to generate high-resolution and low-resolution distilled datasets respectively, with StyleGAN-XL as the deep generative network. To ensure a fair comparison, we maintain consistency by adopting the same network architecture and employing identical hyperparameters. Our code is available at <https://github.com/ndhg1213/H-PD>.

4.1. Settings and Implementation Details

Datasets and Network Architectures In this study, we build upon previous research by utilizing CIFAR10 and Tiny-ImageNet [24] as low-resolution dataset, For high-resolution experiments, we choose ImageNet-1K and ten subsets from it. These subsets, each consisting of ten categories, are divided into the training and validation sets. The detailed categories combination can be found in Appendix.

For the surrogate model for dataset distillation, we choose ConvNet-5 [17] as the backbone network for DM, DSA and TESLA. For ImageNet-1K and Tiny-Imagenet, we conduct experiments on SR²L [46] and adopt ResNet-18 [19] as backbone. To evaluate the performance of the synthetic dataset, we employ various models, including ConveNet, AlexNet [23], VGG-11 [39], ResNet-18, and a Vision Transformer model [13] from the DC-BENCH [9] resource. It is important to note that all of these evaluation models are versions specifically tailored for corresponding resolution datasets.

¹<https://georgecazenavette.github.io/glad>

Alg.	Method	ImNet-A	ImNet-B	ImNet-C	ImNet-D	ImNet-E	ImNette	ImWoof	ImNet-Birds	ImNet-Fruits	ImNet-Cats
TESLA	Pixel	51.7±0.2	53.3±1.0	48.0±0.7	43.0±0.6	39.5±0.9	41.8±0.6	22.6±0.6	37.3±0.8	22.4±1.1	22.6±0.4
	GLaD	50.7±0.4	51.9±1.3	44.9±0.4	39.9±1.7	37.6±0.7	38.7±1.6	23.4±1.1	35.8±1.4	23.1±0.4	26.0±1.1
	H-PD	55.1±0.6	57.4±0.3	49.5±0.6	46.3±0.9	43.0±0.6	45.4±1.1	28.3±0.2	39.7±0.8	25.6±0.7	29.6±1.0
DSA	Pixel	43.2±0.6	47.2±0.7	41.3±0.7	34.3±1.5	34.9±1.5	34.2±1.7	22.5±1.0	32.0±1.5	21.0±0.9	22.0±0.6
	GLaD	44.1±2.4	49.2±1.1	42.0±0.6	35.6±0.9	35.8±0.9	35.4±1.2	22.3±1.1	33.8±0.9	20.7±1.1	22.6±0.8
	H-PD	46.9±0.8	50.7±0.9	43.9±0.7	37.4±0.4	37.2±0.3	36.9±0.8	24.0±0.8	35.3±1.0	22.4±1.1	24.1±0.9
DM	Pixel	39.4±1.8	40.9±1.7	39.0±1.3	30.8±0.9	27.0±0.8	30.4±2.7	20.7±1.0	26.6±2.6	20.4±1.9	20.1±1.2
	GLaD	41.0±1.5	42.9±1.9	39.4±1.7	33.2±1.4	30.3±1.3	32.2±1.7	21.2±1.5	27.6±1.9	21.8±1.8	22.3±1.6
	H-PD	42.8±1.2	44.7±1.3	41.1±1.3	34.8±1.5	31.9±0.9	34.8±1.0	23.9±1.9	29.5±1.5	24.4±2.1	24.2±1.1

Table 1. Synthetic dataset same-architecture performance (%) on ImageNet-Subset (128×128) under IPC=1. "Pixel" refers to not deploying GAN.

Alg.	Method	Tiny-ImageNet		ImageNet-1K	
		IPC-1	IPC-10	IPC-1	IPC-10
SRE ² L	Pixel	2.6±0.1	16.1±0.2	0.1±0.1	21.3±0.6
	GLaD	3.1±0.3	15.7±0.2	1.2±0.1	21.9±0.8
	H-PD	4.5±1.0	18.3±0.5	2.6±0.2	23.5±0.4

Table 2. Synthetic dataset performance comparison with SRE²L on Tiny-ImageNet (64x64) and ImageNet-1K (224x224) evaluated by ResNet-18.

4.2. Performance Improvements

The performance comparison of our method with previous works GLaD is shown in Table 1 and Table 2. We report the same-architecture performance of the synthetic dataset. Since GLaD did not conduct experiments on SRE²L, we chose to adopt the same layers settings (i.e., 12) as TESLA to ensure fairness. compared to optimizing only in a fixed feature space, it can be observed that our method achieves consistent and significant improvements with all the optimization-based methods. This indicates that our method successfully leverages the guidance information provided by all feature domains. The visualized images of synthetic datasets are depicted in Figure 3.

Alg.	Method	ImNet-A	ImNet-B	ImNet-C	ImNet-D	ImNet-E
DSA	Pixel	52.3±0.7	45.1±8.3	40.1±7.6	36.1±0.4	38.1±0.4
	GLaD	53.1±1.4	50.1±0.6	48.9±1.1	38.9±1.0	38.4±0.7
	H-PD	54.1±1.2	52.0±1.1	49.5±0.8	39.8±0.7	40.1±0.7
DM	Pixel	52.6±0.4	50.6±0.5	47.5±0.7	35.4±0.4	36.0±0.5
	GLaD	52.8±1.0	51.3±0.6	49.7±0.4	36.4±0.4	38.6±0.7
	H-PD	55.1±0.5	54.2±0.5	50.8±0.4	37.6±0.6	39.9±0.7

Table 3. Synthetic dataset cross-architecture performance (%) on ImageNet-Subset under IPC=10.

4.3. More Comparisons with GLaD

To align the proposed H-PD with GLaD on higher IPC, i.e. only IPC = 10 under DSA and DM is reported from original paper, our current confirmatory trials achieves a performance improvement of 1% to 3% compared to GLaD with

IPC = 10 under DSA and DM as shown in Table 3, respectively, which demonstrates the effectiveness of H-PD.

Alg.	Method	ConvNet	AlexNet	ResNet-18	VGG-11	ViT
TESLA	Pixel	46.3±0.8	26.8±0.6	23.4±1.3	24.9±0.8	21.2±0.4
	GLaD	35.5±0.6	27.9±0.6	30.2±0.6	31.3±0.7	22.7±0.4
	H-PD	37.2±0.4	28.5±0.3	31.4±0.4	32.2±0.2	24.1±0.4
DSA	Pixel	28.3±0.3	25.9±0.2	27.3±0.5	28.0±0.5	22.9±0.3
	GLaD	29.2±0.8	26.0±0.7	27.6±0.6	28.2±0.6	23.4±0.2
	H-PD	30.2±0.5	26.6±0.4	28.2±0.4	28.0±0.6	24.4±0.5
DM	Pixel	26.0±0.6	22.9±0.2	22.2±0.7	23.8±0.5	21.3±0.5
	GLaD	27.1±0.7	25.1±0.5	22.5±0.7	24.8±0.8	23.0±0.1
	H-PD	27.6±0.7	27.5±0.6	25.6±0.6	25.4±0.8	23.6±0.5

Table 4. Performance(%) across different models on CIFAR-10.

The cross-architecture performance on CIFAR-10 [22] is shown in Table 4. The results demonstrate that using a shallower StyleGAN-XL structure on the lower-resolution dataset CIFAR-10, H-PD still improves the performance of synthetic datasets distilled by different distillation methods. Please note that the released code of GLaD does not include the data augmentation and hyperparameter settings used by TESLA on CIFAR10, which leads to a poor performance on ConvNet.

To present a more comprehensive comparison, we assess the performance of the synthetic dataset across different architectures as shown in Table 5. The cross-architecture accuracy is calculated by averaging the performance of the remaining four models, excluding the backbone model. The results of previous studies are acquired directly from the original papers.

Alg.	Method	ImNet-A	ImNet-B	ImNet-C	ImNet-D	ImNet-E
TESLA	Pixel	33.4±1.5	34.0±3.4	31.4±3.4	27.7±2.7	24.9±1.8
	GLaD	39.9±1.2	39.4±1.3	34.9±1.1	30.4±1.5	29.0±1.1
	H-PD	40.2±0.3	39.8±0.8	35.8±0.7	31.2±1.0	29.5±0.7
DSA	Pixel	38.7±4.2	38.7±1.0	33.3±1.9	26.4±1.1	27.4±0.9
	GLaD	41.8±1.7	42.1±1.2	35.8±1.4	28.0±0.8	29.3±1.3
	H-PD	42.4±1.2	42.6±1.1	36.1±1.1	28.7±1.1	29.6±0.9
DM	Pixel	27.2±1.2	24.4±1.1	23.0±1.4	18.4±0.7	17.7±0.9
	GLaD	31.6±1.4	31.3±3.9	26.9±1.2	21.5±1.0	20.4±0.8
	H-PD	34.9±2.1	33.8±2.0	27.8±1.7	23.6±1.5	22.5±1.3

Table 5. Synthetic dataset cross-architecture performance (%) on ImageNet-Subset.

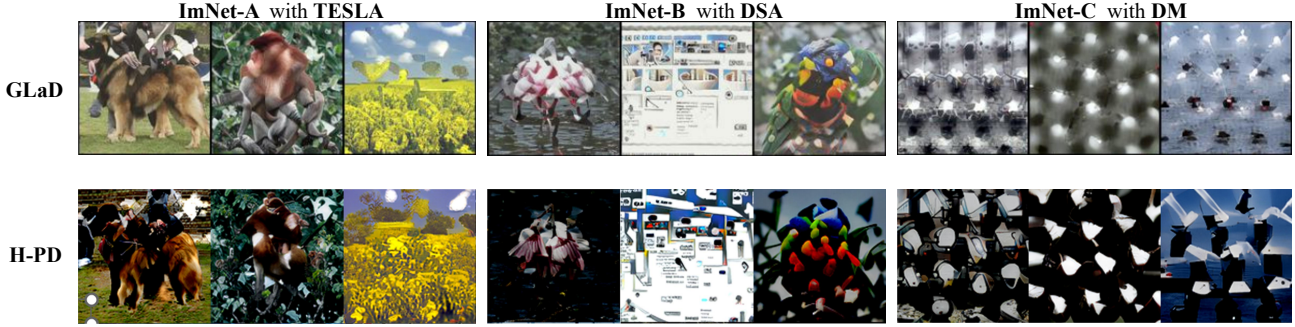


Figure 3. Visualization comparison of the synthetic datasets with different distillation methods.

4.4. Comparison with Diffusion Model Based Methods

Other generative distillation methods consider diffusion as an image generator rather than parameterization methods. Minimax [18] and D⁴M [40] fine-tune the diffusion model and corresponding latent respectively to generate entirely new samples. However, these methods only achieve random sampling outcomes under a high compression ratio (e.g., IPC=1/10). Contrary to these diffusion-based methods, our method in conjunction with GLaD belongs to an optimization-based method, which can effectively accomplish distillation in a more efficient way.

For a fair comparison, we adhere to GLaD’s experimental setting (e.g., a 128x128 resolution image corresponds to a one-hot label), disregarding training time matching [37] and mixiup [47] strategy. As shown in Table 6, our method demonstrates significant advantages at a mechanism compression ratio of IPC=1 without requiring fine-tuning of the pre-trained model.

Method	ImNette	ImWoof	ImNet-Birds	ImNet-Fruits	ImNet-Cats
Minimax	22.8±0.5	17.8±0.3	23.2±0.7	17.5±0.5	19.8±0.3
D ⁴ M	15.2±0.5	17.4±0.6	18.2±0.4	17.6±0.6	23.4±0.7
H-PD	45.4±1.1	28.3±0.2	39.7±0.8	25.6±0.7	29.6±1.0

Table 6. Comparison with generative dataset distillation methods on ImageNet-Subsets under IPC=1.

4.5. Evaluation Protocol

The approach to assessing the performance of a synthetic dataset is as follows: firstly, a set of models is trained using the synthetic dataset. Once the training is complete, the trained models are validated using the corresponding validation set from the real dataset. For a specific model architecture, this process is repeated five times, and the average performance is calculated based on these repetitions. In previous studies, the evaluation method involved continuously optimizing the entire distillation process for 1000 epochs, with sampling the synthetic dataset every 100 epochs. The

Metric	Method	TESLA	DSA	DM
Time	GLaD	75	69	64
	H-PD	70	73	15
performance	GLaD	45.0±0.9	41.3±1.2	37.4±1.6
	H-PD	50.3±0.6	43.2±0.6	39.1±1.2

Table 7. Time complexity (min) and performance (%) averaged on ImageNet-[A, B, C, D, E].

best performance among all sampled examples would then be selected. To ensure a fair comparison, we decompose StyleGAN-XL into $G_{11} \circ \dots \circ G_1 \circ G_0(\cdot)$ and apply the same optimizer and learning rate for each layer, optimizing for 100 steps. This ensures that the total number of optimization epochs remains consistent, thereby preventing performance improvements solely due to a higher number of optimization epochs. The comparison of time complexities and corresponding performance is shown in Table 7. Additionally, we adopt the same setup in our evaluation and sample the synthetic dataset after optimizing for 100 epochs in all of these different feature domains (i.e., \mathbf{z}_i^{K-1}). This approach prevents performance improvements obtained from implicitly selecting a dataset with a higher quality.

Component	ImNet-B	ImNet-C	ImWoof	ImNet-Fruits
GLaD-TESLA	51.9±1.3	44.9±0.4	23.4±1.1	23.1±0.4
+ Average Initialization	53.5±0.7	46.1±0.9	24.8±1.1	22.7±1.2↓
+ Hierarchical Layers	56.2±0.7	48.1±0.9	28.1±1.0	24.1±0.5
+ Distance Metric	57.4±0.3	49.5±0.6	28.3±0.2	25.6±0.7
GLaD-DSA	49.2±1.1	42.0±0.6	22.3±1.1	20.7±1.1
+ Average Initialization	48.9±0.8↓	40.6±0.7↓	22.8±1.4	21.3±1.0
+ Hierarchical Layers	50.1±1.1	43.1±1.4	23.6±0.8	21.9±0.8
+ Distance Metric	50.7±0.9	43.9±0.7	24.0±0.8	22.4±1.1
GLaD-DM	42.9±1.9	39.4±1.7	21.2±1.5	21.8±1.8
+ Average Initialization	43.2±1.6	39.9±1.7	21.1±1.9↓	22.3±1.3
+ Hierarchical Layers	44.2±2.1	41.0±1.2	23.1±0.9	24.1±1.4
+ Distance Metric	44.7±1.3	41.1±1.3	23.9±1.9	24.4±2.1

Table 8. Ablation study of each component with different distillation method across various ImageNet-Subset.

4.6. Ablation Studies

Effectiveness of Each Component As Table 8 shows, the two major components of our method, i.e., hierarchical feature domains and class-relevant feature distance both improve the performance across various ImageNet-Subsets with all distillation methods, especially on TESLA. Optimizing in an unfixed feature space can bring significant gains, and on this basis, using class-relevant feature distance for implicit evaluation can yield a slight additional improvement. Please note that using class-relevant feature distance is infeasible without unfixed optimization spaces. Despite Initialization with averaged noise improves the performance of TESLA and DM to some degree, it cannot achieve stable improvement in the performance of the DSA method. We attribute this discrepancy to the inherent inclination towards noise and edge samples in DSA.

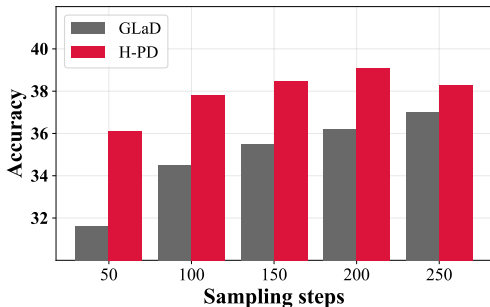


Figure 4. The comparison of performance(%) at the same optimization epoch.

Steps	TESLA	DSA	DM
20	46.9±1.2	39.8±1.1	39.1±1.2
50	47.2±0.8	41.6±0.8	37.0±1.7
100	50.3±0.6	43.2±0.6	36.5±1.4
200	50.5±0.4	43.0±0.6	35.8±1.1

Table 9. Ablation results of optimization steps per optimization space averaged on ImageNet-[A, B, C, D, E].

Optimization Steps We perform 100 optimization steps in each layer to align with the sampling method in previous works. We conduct more experiments across different optimization steps to explore the correct optimization steps. By observing the results shown in Table 9, we find that optimization steps beyond 100 do not yield significant performance improvements for TESLA and DSA methods. Meanwhile, optimization steps below 100 result in performance degradation. Considering the trade-off between effects and costs, we set the steps at 100 for both TESLA and DSA. For DM, however, optimal performance is attained at the least number of steps per layer, i.e., 20 steps. We compare the performance of GLaD and H-PD at the same epoch as

shown in Figure 4, our method outperforms and converges faster, demonstrating the superiority of the approach in utilizing the hierarchical features.

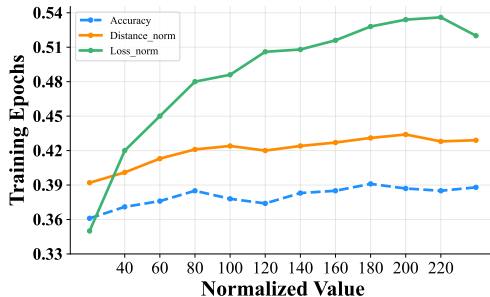


Figure 5. The relationship between searching basis and performance. Note that higher loss-norm values indicate lower loss values and the same applies to feature distances.

Searching Basis To avoid the time-consuming task of directly evaluating the synthetic dataset, we opt for class-relevant feature distance for implicit searching. Specifically, we evaluate the synthetic dataset at specific epochs during the optimization process and subsequently record its ground-truth performance, loss value, and feature distance. Figure 5 demonstrates the recorded values during the optimization process. We normalize the loss values and feature distance to range $[0, 1]$ for clear clarity and comparison. Our observation indicates that compared with the loss value, the feature distance consistently exhibits a stronger negative correlation with the performance.

5. Conclusion

In this paper, we present a novel approach to dataset distillation by exploring hierarchical parameterization space and successfully enhance the GAN-based parameterization method. Our method transforms the optimization space from a specific GAN feature domain to a broader feature space, addressing challenges seen in previous GAN-based parameterization methods. An advantage is that our approach provides a new insight for parameterization methods. Additionally, we anticipate that further improvements can be achieved through detailed optimization steps and optimization space combinations. The proposed H-PD re-explores and showcases the potential of hierarchical features in parameterization distillation for enhancing the performance under extreme compression ratios, contributing to an advanced dataset distillation approach.

Acknowledgement. This work is supported in part by the National Natural Science Foundation of China under grant 62171248, 62301189, Peng Cheng Laboratory (PCL2023A08), and Shenzhen Science and Technology Program under Grant KJZD20240903103702004, JCYJ20220818101012025, RCBS20221008093124061, GXWD20220811172936001.

References

- [1] Ondrej Bohdal, Yongxin Yang, and Timothy Hospedales. Flexible dataset distillation: Learn labels instead of images. *arXiv preprint arXiv:2006.08572*, 2020. 2
- [2] Andrew Brock, Theodore Lim, James M Ritchie, and Nick Weston. Neural photo editing with introspective adversarial networks. *arXiv preprint arXiv:1609.07093*, 2016. 3
- [3] Tom Brown, Benjamin Mann, Nick Ryder, Melanie Subbiah, Jared D Kaplan, Prafulla Dhariwal, Arvind Neelakantan, Pranav Shyam, Girish Sastry, Amanda Askell, et al. Language models are few-shot learners. *Advances in neural information processing systems*, 33:1877–1901, 2020. 1
- [4] George Cazenavette, Tongzhou Wang, Antonio Torralba, Alexei A Efros, and Jun-Yan Zhu. Dataset distillation by matching training trajectories. In *Proceedings of the IEEE/CVF Conference on Computer Vision and Pattern Recognition*, pages 4750–4759, 2022. 2, 3, 4, 11, 17
- [5] George Cazenavette, Tongzhou Wang, Antonio Torralba, Alexei A Efros, and Jun-Yan Zhu. Generalizing dataset distillation via deep generative prior. In *Proceedings of the IEEE/CVF Conference on Computer Vision and Pattern Recognition*, pages 3739–3748, 2023. 1, 2, 3, 4, 12, 17
- [6] Lucy Chai, Jonas Wulff, and Phillip Isola. Using latent space regression to analyze and leverage compositionality in gans. *arXiv preprint arXiv:2103.10426*, 2021. 3
- [7] Mingyang Chen, Jiawei Du, Bo Huang, Yi Wang, Xiaobo Zhang, and Wei Wang. Influence-guided diffusion for dataset distillation. In *The Thirteenth International Conference on Learning Representations*, 2025. 12
- [8] Antonia Creswell, Tom White, Vincent Dumoulin, Kai Arulkumaran, Biswa Sengupta, and Anil A Bharath. Generative adversarial networks: An overview. *IEEE signal processing magazine*, 35(1):53–65, 2018. 3
- [9] Justin Cui, Ruochen Wang, Si Si, and Cho-Jui Hsieh. Dc-bench: Dataset condensation benchmark. *Advances in Neural Information Processing Systems*, 35:810–822, 2022. 5, 17
- [10] Justin Cui, Ruochen Wang, Si Si, and Cho-Jui Hsieh. Scaling up dataset distillation to imagenet-1k with constant memory. In *International Conference on Machine Learning*, pages 6565–6590. PMLR, 2023. 2
- [11] Jia Deng, Wei Dong, Richard Socher, Li-Jia Li, Kai Li, and Li Fei-Fei. Imagenet: A large-scale hierarchical image database. In *2009 IEEE conference on computer vision and pattern recognition*, pages 248–255. Ieee, 2009. 5, 17
- [12] Jacob Devlin, Ming-Wei Chang, Kenton Lee, and Kristina Toutanova. Bert: Pre-training of deep bidirectional transformers for language understanding. *arXiv preprint arXiv:1810.04805*, 2018. 1
- [13] Alexey Dosovitskiy, Lucas Beyer, Alexander Kolesnikov, Dirk Weissenborn, Xiaohua Zhai, Thomas Unterthiner, Mostafa Dehghani, Matthias Minderer, Georg Heigold, Sylvain Gelly, et al. An image is worth 16x16 words: Transformers for image recognition at scale. *arXiv preprint arXiv:2010.11929*, 2020. 1, 5, 17
- [14] Hao Fang, Bin Chen, Xuan Wang, Zhi Wang, and Shu-Tao Xia. Gifd: A generative gradient inversion method with feature domain optimization. In *Proceedings of the IEEE/CVF International Conference on Computer Vision*, pages 4967–4976, 2023. 3
- [15] Hao Fang, Jiawei Kong, Wenbo Yu, Bin Chen, Jiawei Li, Shutao Xia, and Ke Xu. One perturbation is enough: On generating universal adversarial perturbations against vision-language pre-training models. *arXiv preprint arXiv:2406.05491*, 2024.
- [16] Hao Fang, Yixiang Qiu, Hongyao Yu, Wenbo Yu, Jiawei Kong, Baoli Chong, Bin Chen, Xuan Wang, and Shu-Tao Xia. Privacy leakage on dnns: A survey of model inversion attacks and defenses. *arXiv preprint arXiv:2402.04013*, 2024. 3
- [17] Spyros Gidaris and Nikos Komodakis. Dynamic few-shot visual learning without forgetting. In *Proceedings of the IEEE conference on computer vision and pattern recognition*, pages 4367–4375, 2018. 5
- [18] Jianyang Gu, Saeed Vahidian, Vyacheslav Kungurtsev, Haonan Wang, Wei Jiang, Yang You, and Yiran Chen. Efficient dataset distillation via minimax diffusion. In *Proceedings of the IEEE/CVF Conference on Computer Vision and Pattern Recognition*, pages 15793–15803, 2024. 2, 3, 7, 12
- [19] Kaiming He, Xiangyu Zhang, Shaoqing Ren, and Jian Sun. Deep residual learning for image recognition. In *Proceedings of the IEEE conference on computer vision and pattern recognition*, pages 770–778, 2016. 1, 5, 17
- [20] Jeremy Howard. A smaller subset of 10 easily classified classes from imagenet, and a little more french. URL <https://github.com/fastai/imagenette>, 2019. 17
- [21] Jang-Hyun Kim, Jinuk Kim, Seong Joon Oh, Sangdoon Yun, Hwanjun Song, Joonhyun Jeong, Jung-Woo Ha, and Hyun Oh Song. Dataset condensation via efficient synthetic-data parameterization. In *International Conference on Machine Learning*, pages 11102–11118. PMLR, 2022. 3, 11
- [22] A Krizhevsky. Learning multiple layers of features from tiny images. *Master's thesis, University of Tront*, 2009. 5, 6, 17
- [23] Alex Krizhevsky, Ilya Sutskever, and Geoffrey E Hinton. Imagenet classification with deep convolutional neural networks. *Advances in neural information processing systems*, 25, 2012. 5, 17
- [24] Ya Le and Xuan Yang. Tiny imagenet visual recognition challenge. *CS 231N*, 7(7):3, 2015. 5
- [25] Saehyung Lee, Sanghyuk Chun, Sangwon Jung, Sangdoon Yun, and Sungroh Yoon. Dataset condensation with contrastive signals. In *International Conference on Machine Learning*, pages 12352–12364. PMLR, 2022. 2
- [26] Shiye Lei and Dacheng Tao. A comprehensive survey to dataset distillation. *arXiv preprint arXiv:2301.05603*, 2023. 1
- [27] Songhua Liu, Kai Wang, Xingyi Yang, Jingwen Ye, and Xinchao Wang. Dataset distillation via factorization. *Advances in Neural Information Processing Systems*, 35:1100–1113, 2022. 1, 3, 11
- [28] Yanbin Liu, Makoto Yamada, Yao-Hung Hubert Tsai, Tam Le, Ruslan Salakhutdinov, and Yi Yang. Lsmi-sinkhorn: Semi-supervised mutual information estimation with optimal transport. In *Machine Learning and Knowledge Discovery in*

- Databases. Research Track: European Conference, ECML PKDD 2021, Bilbao, Spain, September 13–17, 2021, Proceedings, Part 1 21*, pages 655–670. Springer, 2021. 4
- [29] Yanqing Liu, Jianyang Gu, Kai Wang, Zheng Zhu, Wei Jiang, and Yang You. Dream: Efficient dataset distillation by representative matching. *arXiv preprint arXiv:2302.14416*, 2023. 5
- [30] Mohammed Bany Muhammad and Mohammed Yeasin. Eigen-cam: Class activation map using principal components. In *2020 international joint conference on neural networks (IJCNN)*, pages 1–7. IEEE, 2020. 5, 13
- [31] Timothy Nguyen, Zhoung Chen, and Jaehoon Lee. Dataset meta-learning from kernel ridge-regression. *arXiv preprint arXiv:2011.00050*, 2020. 2
- [32] Timothy Nguyen, Roman Novak, Lechao Xiao, and Jaehoon Lee. Dataset distillation with infinitely wide convolutional networks. *Advances in Neural Information Processing Systems*, 34:5186–5198, 2021. 2
- [33] Yixiang Qiu, Hao Fang, Hongyao Yu, Bin Chen, MeiKang Qiu, and Shu-Tao Xia. A closer look at gan priors: Exploiting intermediate features for enhanced model inversion attacks. In *European Conference on Computer Vision*, pages 109–126. Springer, 2024. 3
- [34] Robin Rombach, Andreas Blattmann, Dominik Lorenz, Patrick Esser, and Björn Ommer. High-resolution image synthesis with latent diffusion models. In *Proceedings of the IEEE/CVF conference on computer vision and pattern recognition*, pages 10684–10695, 2022. 2
- [35] Ahmad Sajedi, Samir Khaki, Ehsan Amjadian, Lucy Z Liu, Yuri A Lawryshyn, and Konstantinos N Plataniotis. Datadam: Efficient dataset distillation with attention matching. In *Proceedings of the IEEE/CVF International Conference on Computer Vision*, pages 17097–17107, 2023. 2
- [36] Axel Sauer, Katja Schwarz, and Andreas Geiger. Stylegan-xl: Scaling stylegan to large diverse datasets. In *ACM SIGGRAPH 2022 conference proceedings*, pages 1–10, 2022. 3
- [37] Zhiqiang Shen and Eric Xing. A fast knowledge distillation framework for visual recognition. In *European conference on computer vision*, pages 673–690. Springer, 2022. 7
- [38] DongHyeok Shin, Seungjae Shin, and Il-chul Moon. Frequency domain-based dataset distillation. In *Thirty-seventh Conference on Neural Information Processing Systems*, 2023. 1, 2, 3, 12
- [39] Karen Simonyan and Andrew Zisserman. Very deep convolutional networks for large-scale image recognition. *arXiv preprint arXiv:1409.1556*, 2014. 5, 17
- [40] Duo Su, Junjie Hou, Weizhi Gao, Yingjie Tian, and Bowen Tang. D⁴: Dataset distillation via disentangled diffusion model. In *Proceedings of the IEEE/CVF Conference on Computer Vision and Pattern Recognition*, pages 5809–5818, 2024. 2, 3, 7, 12
- [41] Ayush Tewari, Mohamed Elgharib, Florian Bernard, Hans-Peter Seidel, Patrick Pérez, Michael Zollhöfer, and Christian Theobalt. Pie: Portrait image embedding for semantic control. *ACM Transactions on Graphics (TOG)*, 39(6):1–14, 2020. 3
- [42] Dmitry Ulyanov, Andrea Vedaldi, and Victor Lempitsky. Instance normalization: The missing ingredient for fast stylization. *arXiv preprint arXiv:1607.08022*, 2016. 17
- [43] Kai Wang, Bo Zhao, Xiangyu Peng, Zheng Zhu, Shuo Yang, Shuo Wang, Guan Huang, Hakan Bilen, Xinchao Wang, and Yang You. Cafe: Learning to condense dataset by aligning features. In *Proceedings of the IEEE/CVF Conference on Computer Vision and Pattern Recognition*, pages 12196–12205, 2022. 2
- [44] Tongzhou Wang, Jun-Yan Zhu, Antonio Torralba, and Alexei A Efros. Dataset distillation. *arXiv preprint arXiv:1811.10959*, 2018. 1, 2, 11
- [45] Weihao Xia, Yulun Zhang, Yujiu Yang, Jing-Hao Xue, Bolei Zhou, and Ming-Hsuan Yang. Gan inversion: A survey. *IEEE Transactions on Pattern Analysis and Machine Intelligence*, 45(3):3121–3138, 2022. 3, 5
- [46] Zeyuan Yin, Eric Xing, and Zhiqiang Shen. Squeeze, recover and relabel: Dataset condensation at imagenet scale from a new perspective. *Advances in Neural Information Processing Systems*, 36, 2024. 5
- [47] Hongyi Zhang, Moustapha Cisse, Yann N Dauphin, and David Lopez-Paz. mixup: Beyond empirical risk minimization. *arXiv preprint arXiv:1710.09412*, 2017. 7
- [48] Bo Zhao and Hakan Bilen. Dataset condensation with differentiable siamese augmentation. In *International Conference on Machine Learning*, pages 12674–12685. PMLR, 2021. 2, 17
- [49] Bo Zhao and Hakan Bilen. Synthesizing informative training samples with gan. *arXiv preprint arXiv:2204.07513*, 2022. 1, 2, 3
- [50] Bo Zhao and Hakan Bilen. Dataset condensation with distribution matching. In *Proceedings of the IEEE/CVF Winter Conference on Applications of Computer Vision*, pages 6514–6523, 2023. 2, 3, 11
- [51] Bo Zhao, Konda Reddy Mopuri, and Hakan Bilen. Dataset condensation with gradient matching. *arXiv preprint arXiv:2006.05929*, 2020. 2, 3, 11
- [52] Xinhao Zhong, Bin Chen, Hao Fang, Xulin Gu, Shu-Tao Xia, and En-Hui Yang. Going beyond feature similarity: Effective dataset distillation based on class-aware conditional mutual information. *arXiv preprint arXiv:2412.09945*, 2024. 13
- [53] Xinhao Zhong, Shuoyang Sun, Xulin Gu, Zhaoyang Xu, Yaowei Wang, Jianlong Wu, and Bin Chen. Efficient dataset distillation via diffusion-driven patch selection for improved generalization. *arXiv preprint arXiv:2412.09959*, 2024. 12
- [54] Yongchao Zhou, Ehsan Nezhadarya, and Jimmy Ba. Dataset distillation using neural feature regression. *Advances in Neural Information Processing Systems*, 35:9813–9827, 2022. 2
- [55] Chenyang Zhu, Kai Li, Yue Ma, Chunming He, and Xiu Li. Multiboost: Towards generating all your concepts in an image from text. *arXiv preprint arXiv:2404.14239*, 2024. 12
- [56] Chenyang Zhu, Kai Li, Yue Ma, Longxiang Tang, Chengyu Fang, Chubin Chen, Qifeng Chen, and Xiu Li. Instantswap: Fast customized concept swapping across sharp shape differences. *arXiv preprint arXiv:2412.01197*, 2024. 12

Hierarchical Features Matter: A Deep Exploration of Progressive Parameterization Method for Dataset Distillation

Supplementary Material

A. Literature Reviews on Dataset Distillation

A.1. Dataset Distillation in Pixel Space

In this section, we review the methodology of optimizing synthetic dataset S with the surrogate objective in pixel space, which provides the basic optimization objective for all parameterization dataset distillation methods.

A.1.1 DC [51].

Dataset Distillation (DD) [44] aims at optimizing the synthetic dataset S with a bi-level optimization. The main idea of bi-level optimization is that a network with parameter θ_S , which is trained on S , should minimize the risk of the real dataset \mathcal{T} . However, due to the need to pass through an unrolled computation graph, DD brings about a significant amount of time overhead. Based on this, DC introduces a surrogate objective, which aims at matching the gradients of a network during the optimization. For a network with parameters θ_S trained on the synthetic data for some number of iterations, the matching loss is

$$\mathcal{L}_{DC} = 1 - \frac{\nabla_{\theta} \ell^S(\theta) \cdot \nabla_{\theta} \ell^T(\theta)}{\|\nabla_{\theta} \ell^S(\theta)\| \|\nabla_{\theta} \ell^T(\theta)\|}, \quad (7)$$

where $\ell^T(\cdot)$ represents the loss function (e.g., CE loss) calculated on real dataset \mathcal{T} , and $\ell^S(\cdot)$ is the same loss function calculated on synthetic dataset \mathcal{T} .

A.1.2 DM [50].

Despite DC significantly reducing time consumption through surrogate, bi-level optimization still introduces a substantial amount of time overhead, especially when dealing with high-resolution and large-scale datasets. DM achieves this by using only the features extracted from networks ψ with random initialization as the matching target, the matching loss is

$$\mathcal{L}_{DM} = \sum_c \left\| \frac{1}{|\mathcal{T}_c|} \sum_{\mathbf{x} \in \mathcal{T}_c} \psi(\mathbf{x}) - \frac{1}{|\mathcal{S}_c|} \sum_{\mathbf{s} \in \mathcal{S}_c} \psi(\mathbf{s}) \right\|^2, \quad (8)$$

where \mathcal{T}_c and \mathcal{S}_c represents the real and synthetic images from class c respectively.

A.1.3 MTT [4].

Distinct from the short-range optimization introduced from DC, MTT utilizes many expert trajectories $\{\theta_t^*\}_{t=0}^T$ which are

obtained by training networks from scratch on the full real dataset and choose the parameter distance the matching objective. During the distillation process, a student network is initialized with parameters θ_t^* by sample expert trajectory at timestamp t and then trained on the synthetic data for some number of iterations N , the matching loss is

$$\mathcal{L}_{MTT} = \frac{\|\hat{\theta}_{t+N} - \theta_{t+M}^*\|^2}{\|\theta_t^* - \theta_{t+M}^*\|^2}, \quad (9)$$

where θ_{t+M}^* represents the expert trajectory at timestamp $t + M$.

A.2. Dataset Distillation in Feature Domain

In this section, we review the methodology of parameterization dataset distillation built upon the aforementioned dataset distillation methods, achieving better performance by employing a differentiable operation $\mathcal{F}(\cdot)$ to shift the optimization space from pixel space to various feature domain, which can be formulated as

$$\mathcal{S} = \{\mathcal{F}(\mathbf{z})\}. \quad (10)$$

where \mathbf{z} represents latent code in the feature domain corresponding to $\mathcal{F}(\cdot)$.

A.2.1 HaBa [27].

HaBa breaks the synthetic dataset into bases and a small neural network called hallucinator which is utilized to produce additional synthetic images. By leveraging this technique, the resulting model could be regarded as a differentiable operation and produce more diverse samples. However, HaBa simultaneously optimizes the bases and the hallucinator, neglecting the relationship between the two feature domains. This leads to unstable optimization during the training process.

A.2.2 IDC [21].

IDC proposes a principle that small-sized synthetic images often carry more effective information under the same spatial budget and utilize an upsampling module as the differentiable operation. Despite employing a differentiable operation, the optimization of IDC is still the pixel space, which resulted in the loss of effective information gain obtained from other feature domains.

A.2.3 FreD [38].

FreD suggests that optimizing for the main subject in the synthetic image is more instructive than optimizing for all the details. Therefore, FreD employs discrete cosine transform (DCT) as the differentiable operation and uses a learnable mask matrix to remove high-frequency information, ensuring that the optimization process only occurs in the low-frequency domain. This allows the synthetic dataset to achieve higher performance and generalization. However, FreD overlooks the effective guiding information within the high-frequency domain and fails to connect the two feature domains produced by DCT, leading to potential incomplete optimization.

A.2.4 GLaD [5].

Different from existing methods [7, 18, 40, 53] utilizing diffusion models [55, 56], GLaD employs a pre-trained generative model (i.e., GAN) and distills the synthetic dataset in the corresponding latent space. By leveraging the capability of a generative model to map latent noise to image patterns, GLaD achieves better generalization to unseen architecture and scale to high-dimensional datasets. However, for StyleGAN, the earlier layers tend to provide the information about the main subject in an image while the later layers often contribute to the details. However, GLaD attempts to balance the low-frequency information with the high-frequency information by selecting an intermediate layer as a fixed optimization space, discarding the guiding information from the earlier layers can lead to incomplete optimization. Another limitation of GLaD is the need for a large number of preliminary experiments. GLaD selects a specific intermediate layer suitable for all datasets for different distillation methods. However, under the same distillation method, the optimal intermediate layer corresponding to different datasets is not the same, especially when the manifold of the datasets varies greatly, which suggests that GLaD cannot spontaneously adapt to different datasets, distillation methods, and GANs.

B. Additional Experimental Results

B.1. More Comparisons with GLaD

To expand the optimization space, the method we proposed utilizes hierarchical feature domains composed of intermediate layers from GAN. To investigate whether optimization across multiple feature domains is superior to optimization within a single fixed feature domain, we evaluate the performance by simply expanding the optimization space based on the baseline. As shown in Table 10, compared to GLaD, which only selects a single yet optimal intermediate layer of the GAN as the optimization space, H-PD has successfully

achieved considerable improvement, validating our viewpoint that the optimization result from the previous feature domain can serve as better starting point for subsequent feature domain. Please note the result is obtained by not selecting \mathcal{S}^* .

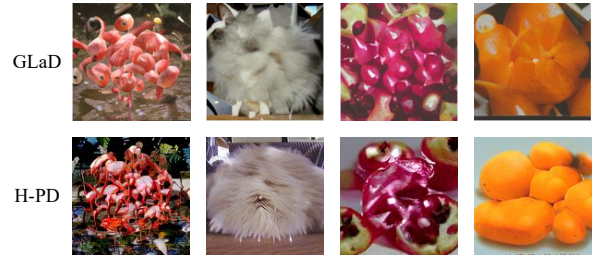


Figure 6. The comparison of visualization.

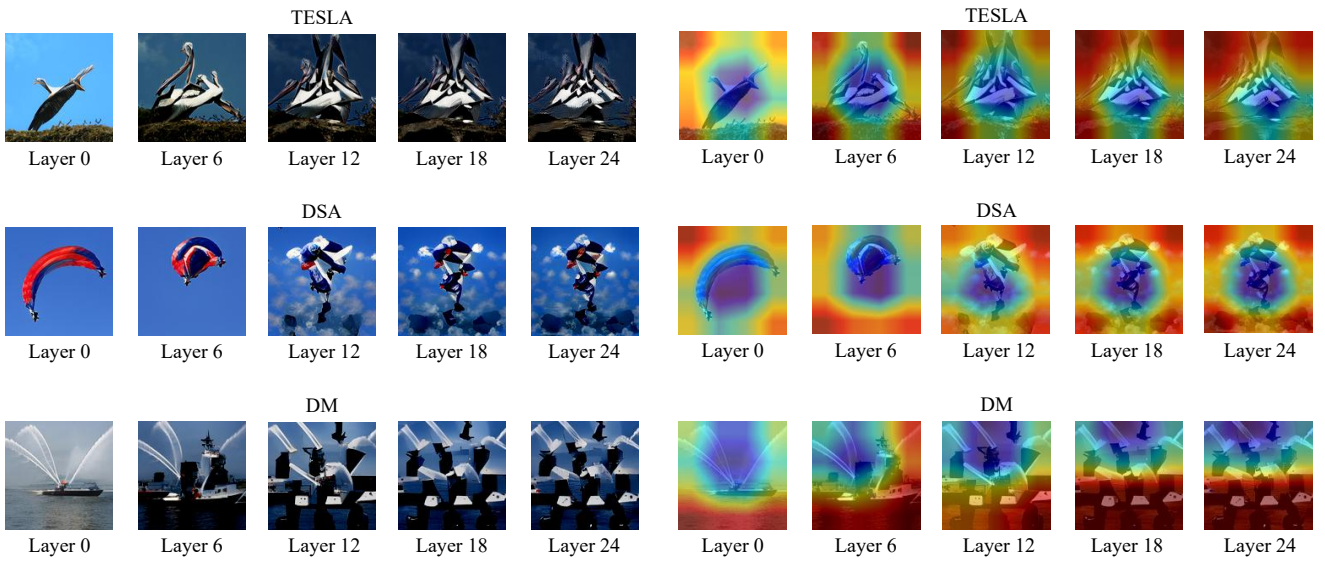
To present a more comprehensive comparison, we evaluate the cross-architecture performance of a high-resolution synthetic dataset under the same setting (i.e., DSA on ImageNet-[A, B, C, D, E] under IPC=1). As shown in Table 11, our proposed H-PD still achieves considerable improvements, demonstrating the stability of our proposed method. Figure 6 illustrates the comparison of synthetic dataset visualization generated by H-PD and GLaD using the same initial image. The images produced by H-PD achieve a good balance between content and style. On one hand, H-PD tends to preserve more main subject information by optimizing in the earlier layers of the GAN. On the other hand, since H-PD also undergoes optimization in the later layers, the synthetic images tend to be sharper and rarely produce the kaleidoscope-like patterns that are common in the GLaD method.

B.2. Visualizing Morphological Transition of Synthetic Images

As shown in Figure 7a, we demonstrate the visualization changes of the synthetic image throughout the optimization process. Layer 0 represents the initial image produced by StyleGAN-XL using averaged noise, and Layer i indicates the image when the optimization space reaches layer i . In the early stage of optimization, since the optimization space is located in the earlier layer of the GAN, the optimization object primarily focus on the main subject of the synthetic image. Meanwhile, GAN still maintains a high degree of integrity which leads to a strong constraint on the slight changes in the latent produced during the optimization process, which can be transformed into patterns resembling real images instead of noises. Thus the tendency in the early stage of optimization is to generate images that better conform to the constraint of distillation loss yet appear more realistic, leading to produce synthetic images that can be regarded as a better starting point for the subsequent

Alg.	Opimization Space	ImNet-A	ImNet-B	ImNet-C	ImNet-D	ImNet-E	ImNette	ImWoof	ImNet-Birds	ImNet-Fruits	ImNet-Cats
TESLA	Fixed (Pixel)	51.7±0.2	53.3±1.0	48.0±0.7	43.0±0.6	39.5±0.9	41.8±0.6	22.6±0.6	37.3±0.8	22.4±1.1	22.6±0.4
	Fixed (GAN)	50.7±0.4	51.9±1.3	44.9±0.4	39.9±1.7	37.6±0.7	38.7±1.6	23.4±1.1	35.8±1.4	23.1±0.4	26.0±1.1
	Unfixed	53.1±0.8	55.4±0.7	47.5±0.9	44.1±0.6	40.8±0.7	42.8±1.0	27.0±0.6	37.6±0.9	24.7±0.7	28.3±0.8
DSA	Fixed (Pixel)	43.2±0.6	47.2±0.7	41.3±0.7	34.3±1.5	34.9±1.5	34.2±1.7	22.5±1.0	32.0±1.5	21.0±0.9	22.0±0.6
	Fixed (GAN)	44.1±2.4	49.2±1.1	42.0±0.6	35.6±0.9	35.8±0.9	35.4±1.2	22.3±1.1	33.8±0.9	20.7±1.1	22.6±0.8
	Unfixed	46.1±0.7	50.0±0.9	43.8±1.4	37.1±0.9	36.6±0.6	36.2±0.5	22.7±0.3	34.9±1.5	21.2±0.8	23.1±0.3
DM	Fixed (Pixel)	39.4±1.8	40.9±1.7	39.0±1.3	30.8±0.9	27.0±0.8	30.4±2.7	20.7±1.0	26.6±2.6	20.4±1.9	20.1±1.2
	Fixed (GAN)	41.0±1.5	42.9±1.9	39.4±1.7	33.2±1.4	30.3±1.3	32.2±1.7	21.2±1.5	27.6±1.9	21.8±1.8	22.3±1.6
	Unfixed	42.3±1.5	44.1±1.5	41.3±1.7	33.7±1.1	31.5±1.1	34.0±1.2	23.1±1.3	28.9±1.4	24.3±1.3	22.8±0.8

Table 10. Abltion study on optimization space comparison. "Fixed (Pixel)" refers to optimize in pixel space and "Fixed (GAN)" refers to GLaD, while Unfixed refers to optimize in multiple feature domains.



(a) Visualization of synthetic images.

(b) Visualization of corresponding CAM.

Figure 7. The visualization change of synthetic images and corresponding CAM during the optimization process using different distillation methods. "Layer" refers to the index of intermediate layers provided by StyleGAN-XL.

Method	ImNet-A	ImNet-B	ImNet-C	ImNet-D	ImNet-D
Pixel	38.3±4.7	32.8±4.1	27.6±3.3	25.5±1.2	23.5±2.4
GLaD	37.4±5.5	41.5±1.2	35.7±4.0	27.9±1.0	29.3±1.2
H-PD	40.7±2.1	42.9±1.8	37.2±2.2	30.1±1.7	29.7±1.8

Table 11. Higher-resolution (256×256) synthetic dataset (using DSA) cross-architecture performance (%).

optimization process.

In the later stage of optimization, the main subject of the synthetic image no longer undergoes significant changes, and the optimization objective shifts along with the movement of the optimization space, focusing more on the details of the synthetic images. As shown in Figure 7a, due

to the weakened generative constraint of the incomplete GAN, the final synthetic image becomes similar to the indistinguishable and distorted image produced by existing distillation methods. Building upon the better synthetic image obtained through the optimization process in the earlier layers, different distillation methods gradually incorporate more guidance-oriented customized patterns into the synthetic image, achieving further performance improvement, which has also been proved by recent work [52].

B.3. Qualitative Interpretation using CAM

We additionally introduce CAM [30] to visualize the heatmap of class-relevant information in the synthetic images as shown in Figure 7b, which also demonstrates our perspective from another aspect. The blue areas represent

Layers	Optimization	ImNet-A	ImNet-B	ImNet-C	ImNet-D	ImNet-E	ImNette	ImWoof	ImNet-Birds	ImNet-Fruits	ImNet-Cats
1	50	53.6±0.2	55.2±1.5	47.3±0.5	44.1±0.7	40.5±1.1	43.8±0.4	26.6±0.7	37.1±0.6	22.9±0.5	27.8±1.0
	100	55.3±0.8	57.1±0.7	49.1±0.9	46.6±0.4	42.2±1.5	44.9±1.2	28.6±0.6	39.4±0.8	25.9±0.7	30.1±1.2
	200	55.4±0.7	57.5±1.1	48.6±0.8	46.2±0.9	43.6±0.6	45.7±0.5	28.7±0.4	39.4±0.6	25.5±0.5	29.8±0.2
2	50	51.3±0.9	54.2±1.1	46.3±0.8	44.1±1.2	40.3±1.2	41.8±1.4	27.1±0.6	36.5±1.1	23.0±1.2	28.1±1.3
	100	55.1±0.6	57.4±0.3	49.5±0.6	46.3±0.9	43.0±0.6	45.4±1.1	28.3±0.2	39.7±0.8	25.6±0.7	29.6±1.0
	200	55.6±0.9	57.9±0.5	49.4±0.3	46.0±0.1	43.5±0.4	45.1±0.7	28.6±0.2	39.3±0.8	25.9±1.1	29.9±0.6
4	50	51.8±0.7	52.9±1.2	46.1±1.5	42.3±0.5	39.8±0.5	40.9±1.3	24.7±1.1	35.9±0.5	21.2±1.7	25.3±1.1
	100	53.3±0.8	54.2±1.1	47.3±1.2	41.8±1.7	42.7±0.6	27.7±0.5	27.1±1.0	27.0±0.9	22.5±1.4	26.4±1.2
	200	55.0±1.0	57.0±1.3	48.1±1.6	45.2±0.5	42.1±1.4	45.0±0.5	27.2±0.9	38.8±1.1	24.6±0.5	28.4±0.8

Table 12. Abltion study on layers combination and optimization allocation using TESLA. "Layers" refers to the number of layers per optimization space, "Optimization" refers to the number of SGD steps allocated in each optimization space.

Layers	Optimization	ImNet-A	ImNet-B	ImNet-C	ImNet-D	ImNet-E	ImNette	ImWoof	ImNet-Birds	ImNet-Fruits	ImNet-Cats
1	50	45.2±1.2	48.3±1.3	42.0±0.4	36.2±0.7	35.0±0.8	35.8±1.1	22.7±1.0	33.5±0.5	21.1±1.5	22.7±0.8
	100	46.2±0.7	51.1±0.4	43.3±1.1	37.2±0.5	36.6±0.9	36.7±1.3	22.9±0.8	35.6±1.1	22.1±1.5	23.8±0.7
	200	46.5±0.9	50.7±1.1	43.8±0.2	37.3±0.7	37.6±0.7	36.9±1.3	24.3±0.5	34.9±0.3	22.6±1.3	23.6±0.7
2	50	44.8±0.4	48.9±0.9	42.1±1.1	35.6±1.0	36.6±0.6	34.2±1.1	22.1±0.6	33.3±1.6	20.0±1.3	22.7±0.8
	100	46.9±0.8	50.7±0.9	43.9±0.7	37.4±0.4	37.2±0.3	36.9±0.8	24.0±0.8	35.3±1.0	22.4±1.1	24.1±0.9
	200	46.8±0.5	50.8±0.3	43.4±0.6	37.0±1.3	37.3±0.5	37.1±0.7	23.8±1.3	35.6±1.1	22.1±1.2	24.6±1.3
4	50	43.6±0.7	47.8±0.7	40.4±0.6	34.6±0.5	34.2±0.8	33.4±1.2	21.3±0.9	32.7±1.4	19.9±0.5	21.6±0.6
	100	45.7±0.7	49.4±0.9	43.1±1.1	36.1±1.3	36.4±0.8	35.2±0.6	23.4±1.1	34.7±0.5	21.3±1.1	23.5±1.3
	200	46.3±0.8	50.1±0.9	43.2±0.7	37.0±0.4	36.8±1.6	36.2±1.0	23.3±1.3	34.4±1.4	21.6±0.8	23.7±0.5

Table 13. Abltion study on layers combination and optimization allocation using DSA.

regions of class-relevant information, which can produce the largest gradient during the training process. Conversely, the red areas indicate regions of class-irrelevant information, with deeper colors signifying higher degrees of corresponding information. In the early stage of optimization, the class-relevant information of the main subject in the synthetic image produced by various distillation methods is compressed.

Interestingly, for the gradient matching methods TESLA and DSA, which rely on long-range and short-range gradient matching respectively, the class-relevant information of the main subject remains unchanged when optimization space changes to later layers, while the gradient that can be produced by the image background (e.g., corners) are further decreased, as indicated by the deeper red color, even though the changes in the background are hardly observable by the naked eye during the optimization process. However, for the feature matching method DM, compared to the visualized kaleidoscope-like pattern, the visualization of corresponding CAM shows an unbalanced distribution and focuses on areas not typically observed by humans. We believe this phenomenon also explains the poorer performance of DM compared with gradient matching methods. Compared to the synthetic images with a centralized concen-

tration of class-relevant information produced by TESLA and DSA, the images generated by DM are too diverse due to fitting all the features of the entire dataset including the class-irrelevant features, which is disadvantageous for training neural networks on tiny distilled datasets.

B.4. Layers Combination and Optimization Allocation

As discussed, we adopt a uniform sampling method that evaluates the synthetic dataset per 100 optimization epochs (even less when using DM) to align with the evaluation method of the baseline (i.e., GLaD). Additionally, we decompose StylGAN-XL into $G_{11} \circ \dots \circ G_1 \circ G_0(\cdot)$ to align with the time complexity of the baseline. We present an ablation study on the allocation of optimization epochs per optimization space. Building on this, we further explore the impact of combining different numbers of intermediate layers into a single optimization space and allocating different numbers of optimization epochs to each optimization space on the performance of the synthetic dataset. For all distillation methods, we explore the impact of varying optimization spaces by using combinations of 1, 2, and 4 intermediate layers within each optimization space. Under the same optimization space setting, for TESLA and DSA, we

investigated the effects of different numbers of optimization epochs allocated to each optimization space by using 50, 100, and 200. For DM, due to the overfitting issue caused by feature matching, we used 10, 20, and 50 as the number of optimization epochs per optimization space.

The results for TESLA and DSA are shown in Table 12 and Table 13. Combining 1 or 2 intermediate layers as a single optimization space does not produce a significant impact on the performance, indicating that existing redundant feature spaces provided by GAN contribute little to the distillation tasks and may even lead to a negative effect. Under this setting, allocating 50 optimization epochs per optimization space produces a clear phenomenon of optimization not converging. However, when the number of optimization epochs comes to 100 or 200, the optimization converges without significant performance differences. Achieved by implicitly selecting the optimal synthetic dataset through the proposed class-relevant feature distance metric, allowing us to avoid overfitting issues to some extent through a certain level of optimization path withdrawal. Therefore, we choose 100 epochs as the basic setting to reduce time complexity in the actual training process. When using 4 intermediate layers as an optimization space, the performance is decreased even when setting optimization epochs to 200, indicating that too few feature domains could not provide sufficiently rich guiding information, forcing the optimization process to require more epochs to converge, demonstrating the superiority of our proposed H-PD in utilizing multiple feature domains.

The results for DM are shown in Table 14. Similar to TESLA and DSA, Combining 1 or 2 intermediate layers as a single optimization space results in similar performance, while combining 4 intermediate layers as optimization space leads to a significant performance drop. However, under the same optimization space settings, an excessive number of optimization epochs often leads to a severe decline in performance when using DM as the distillation method. As aforementioned, DM is unable to focus on class-relevant information, which causes an irreversible loss of the main subject information in the synthetic image after deploying a large number of optimization epochs in a specific feature domain, which in turn leads to a situation where the informative guidance provided by subsequent feature domains could not be effectively incorporated into the synthetic image, resulting in performance degradation. In this case, even the proposed class-relevant feature distance could not effectively select a superior synthetic dataset. To align with the approach of decomposing GAN used in TESLA and DSA, we ultimately combine 2 intermediate layers as an optimization space and deploy 20 optimization epochs as the experimental setting for DM.

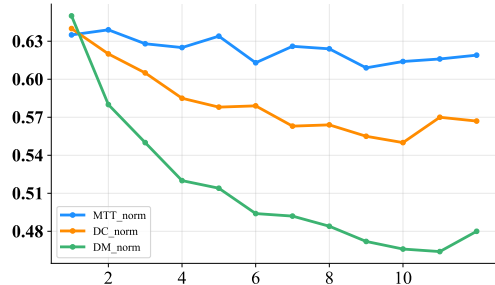


Figure 8. Quantitative results of loss function value using different distillation methods. Note that we normalize all the values for clear comparison.

B.5. Ablation Study on Searching Strategy

To better utilize the informative guidance provided by multiple feature domains, we propose class-relevant feature distance as an evaluation metric for implicitly selecting the optimal synthetic dataset. We demonstrate the ablation study using different implicit evaluation metrics, as shown in Table 15, the metric we proposed outperforms the use of loss function value corresponding to the distillation methods as the metric under all settings. It is worth noting that, although the accuracy of the model trained on the synthetic dataset can be used as an explicit evaluation metric for the data distillation task, the evaluation process incurred much greater time overhead than the distillation task itself, rendering it impractical for actual training processes.

To explore the principle of the superiority of class-relevant feature distance, we first discussed the respective limitations of directly using existing distillation loss function value as the evaluation metric. The tendency of different distillation loss functions is shown in Figure 8. For TESLA, the loss function is obtained by calculating the distance between the student network parameters and the teacher network parameters. However, in order to consider diversity, TESLA selects a random initialization method when initializing the student network parameters, and the expert trajectory also comes from the training process of models with different initialization, leading to a significant fluctuation caused by utilizing different initialization parameters. For DSA, the loss function utilizes neural network gradients as guidance. However, when $IPC=1$, the proxy neural network used in each optimization process is randomly initialized, causing DSA to face the same issue as TESLA, where the loss function is affected by network parameter initialization. As for DM, the loss function is obtained from the feature distance between the dataset features extracted by randomly initialized networks, resulting in the same impact of network initialization parameters on this loss function. Additionally, DM suffers from severe overfitting in the later stages of optimization due to fitting

Layers	Optimization	ImNet-A	ImNet-B	ImNet-C	ImNet-D	ImNet-E	ImNette	ImWoof	ImNet-Birds	ImNet-Fruits	ImNet-Cats
1	10	42.1±2.2	44.1±1.6	41.7±1.7	33.9±1.2	31.3±1.9	34.2±2.1	24.1±1.4	29.7±0.7	24.1±1.6	22.6±1.3
	20	41.6±1.6	44.8±1.8	41.3±1.4	34.1±2.1	31.2±0.5	33.7±0.6	24.0±1.3	29.6±1.7	23.4±0.8	23.7±1.9
	50	40.2±1.6	43.4±1.7	40.2±2.0	33.1±1.3	29.7±1.8	32.6±1.9	23.1±2.1	28.2±1.6	22.1±0.8	21.0±0.5
2	10	41.4±1.7	43.5±1.3	40.4±0.9	34.1±1.3	31.3±1.8	33.6±1.7	22.4±1.6	28.3±2.1	23.1±1.7	22.9±1.5
	20	42.8±1.2	44.7±1.3	41.1±1.3	34.8±1.5	31.9±0.9	34.8±1.0	23.9±1.9	29.5±1.5	24.4±2.1	24.2±1.1
	50	40.1±1.8	42.6±2.0	40.2±1.6	32.6±1.7	29.7±1.3	33.1±0.6	21.6±0.7	27.7±1.6	22.2±1.3	22.4±1.9
4	10	39.9±1.4	42.5±1.0	40.4±1.8	32.4±1.6	30.1±2.4	32.7±2.3	20.9±1.6	27.5±2.2	22.5±1.7	21.8±1.2
	20	40.6±1.3	42.5±1.6	39.6±2.1	32.2±1.5	30.1±1.3	32.9±1.8	21.6±1.5	27.3±1.2	21.7±2.3	22.3±1.6
	50	40.4±1.7	42.7±1.3	39.9±1.2	32.0±1.4	30.3±1.9	32.6±1.6	22.0±1.1	27.8±0.9	21.1±1.7	22.6±1.4

Table 14. Ablation study on layers combination and optimization allocation using DM.

Alg.	Searching Basis	ImNet-A	ImNet-B	ImNet-C	ImNet-D	ImNet-E	ImNette	ImWoof	ImNet-Birds	ImNet-Fruits	ImNet-Cats
TESLA	-	54.7±0.8	56.2±0.7	48.1±0.9	45.4±0.9	41.8±0.6	43.8±0.8	28.1±1.0	38.5±1.2	24.1±0.5	28.7±0.9
	Loss Value	53.6±0.9	56.9±0.7	48.3±0.8	45.0±0.6	41.0±1.2	44.5±0.8	27.5±1.4	37.8±0.7	25.1±0.9	27.6±1.0
	Feature Distance	55.1±0.6	57.4±0.3	49.5±0.6	46.3±0.9	43.0±0.6	45.4±1.1	28.3±0.2	39.7±0.8	25.6±0.7	29.6±1.0
DSA	-	45.9±0.7	50.1±1.1	43.1±1.4	36.9±0.8	36.8±0.6	36.0±0.9	23.6±0.8	34.5±0.4	21.9±0.8	23.2±0.9
	Loss Value	46.6±1.3	48.9±1.7	43.6±1.1	36.1±1.2	36.6±0.5	36.2±0.9	23.1±0.6	33.6±0.7	21.3±1.1	22.8±1.0
	Feature Distance	46.9±0.8	50.7±0.9	43.9±0.7	37.4±0.4	37.2±0.3	36.9±0.8	24.0±0.8	35.3±1.0	22.4±1.1	24.1±0.9
DM	-	42.4±1.6	44.2±2.1	41.0±1.2	34.0±1.2	31.1±1.0	34.5±2.1	23.1±0.9	29.0±1.5	24.1±1.4	22.6±1.5
	Loss Value	41.6±1.8	44.4±1.4	40.7±2.1	34.6±1.7	30.1±1.3	34.5±1.3	23.6±1.2	28.7±1.3	24.4±1.3	21.2±1.2
	Feature Distance	42.8±1.2	44.7±1.3	41.1±1.3	34.8±1.5	31.9±0.9	34.8±1.0	23.9±1.9	29.5±1.5	24.4±2.1	24.2±1.1

Table 15. Quantitative results on searching basis. "-" refers to not employing a searching strategy, "Loss Value" refers to directly using corresponding loss function value as the searching basis, "Feature Distance" refers to the use of proposed class-relevant distance as a searching basis

to the useless features. In summary, the loss functions corresponding to the three distillation methods could not serve as effective evaluation metrics due to the excessive diversity.

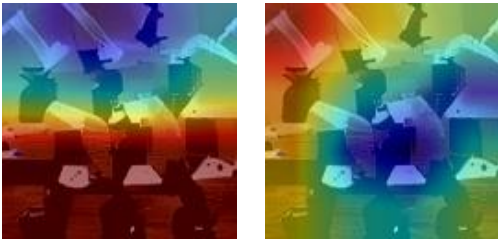


Figure 9. The visualization comparison of CAM between pre-trained model and random model using DM.

Distinguished from existing distillation methods, where the loss function is influenced by the need to fit diversity, our proposed class-relevant feature distance effectively addresses this issue by using CAM, which is calculated by utilizing a pre-trained neural network, and we utilize a ResNet-18 trained on ImageNet-1k as a proxy model for computing CAM. As shown in Figure 9, we demonstrate the difference between the visualization obtained using the pre-trained model and those obtained using a randomly initial-

ized model. The observation indicates that there is a significant difference in the regions of interest for the two, by utilizing a pre-trained model with fixed parameters, we can better identify the feature regions that are beneficial for the classification task (i.e., larger gradients). Therefore, our proposed metric successfully leverages this strong supervisory signal to achieve data selection while eliminating the strong correlation between the loss function and the proxy model parameters.

Method	ImNet-A	ImNet-B	ImNet-C	ImNet-D	ImNet-E
GLaD-TESLA	50.7±0.4	51.9±1.3	44.9±0.4	39.9±1.7	37.6±0.7
+ Average Initialization	51.9±1.0	53.5±0.7	46.1±0.9	41.0±0.7	39.1±1.0
GLaD-DSA	44.1±2.4	49.2±1.1	42.0±0.6	35.6±0.9	35.8±0.9
+ Average Initialization	45.4±0.6	48.9±0.8	40.6±0.7	36.4±0.5	34.8±0.3
GLaD-DM	41.0±1.5	42.9±1.9	39.4±1.7	33.2±1.4	30.3±1.3
+ Average Initialization	41.5±1.2	43.2±1.6	39.9±1.7	32.2±0.9	30.8±1.3

Table 16. Ablation study of average noise initialization on GLaD.

B.6. Ablation Study on Average Noise Initialization

To investigate the effect of using averaged noise as initialization, we conduct ablation experiments on both GLaD and H-PD respectively. As shown in Table 16, averaged noise often provides a significant gain for GLaD. Indicating that

using averaged noise as input tends to produce images with reduced bias that conform to the statistical characteristics of the real dataset, implying that images generated from averaged noise are usually centered within the real dataset. As aforementioned, since GLaD neglects the informative guidance from the earlier layers, leading to a lack of optimization for the main subject of the synthetic image, averaged noise can to some extent replace this operation.

Method	ImNet-A	ImNet-B	ImNet-C	ImNet-D	ImNet-E
H-PD-TESLA	54.1±0.5	56.8±0.4	48.9±1.3	45.0±0.7	42.1±0.6
+ Average Initialization	55.1±0.6	57.4±0.3	49.5±0.6	46.3±0.9	43.0±0.6
H-PD-DSA	46.5±1.0	50.4±0.4	44.5±0.6	37.7±1.1	36.9±0.7
+ Average Initialization	46.9±0.8	50.7±0.9	43.9±0.7	37.4±0.4	37.2±0.3
H-PD-DM	42.6±1.6	44.5±0.9	42.3±1.4	34.5±1.1	32.3±1.3
+ Average Initialization	42.8±1.2	44.7±1.3	41.1±1.3	34.8±1.5	31.9±0.9

Table 17. Ablation study of average noise initialization on H-PD.

As shown in Table 17, average noise initialization provides only a limited improvement for H-PD on TESLA, while using DSA and DM, averaged noise is closer to random initialization. The observation aligns with our perspective that H-PD requires optimization through all layers of the GAN, which has already led to optimization for the main subject information that conforms to the constraints of the loss function during the early stages of training. The role of averaged noise is then reduced to merely providing samples that better conform to statistical characteristics, which is also why we still employ averaged noise for H-PD to obtain a training-free optimization starting point.

Additionally, since DSA tends to optimize towards classification boundary samples or noisy samples, and DM tends to substantially modify synthetic datasets to achieve feature maximum mean discrepancy optimization, neither GLaD nor H-PD with average noise initialization can effectively improve the performance on DSA and DM. Nevertheless, TESLA is most effective in preserving the primary subject information in the synthetic images, which allows for the averaging of noise and the achievement of a relatively stable improvement.

C. Experimental Details

C.1. Dataset

We evaluate H-PD on various datasets, including a low-resolution dataset CIFAR10[22] and a large number of high-resolution datasets ImageNet-Subset.

- CIFAR-10 consists of 32×32 RGB images with 50,000 images for training and 10,000 images for testing. It has 10 classes in total and each class contains 5,000 images for training and 1,000 images for testing.
- ImageNet-Subset is a small dataset that is divided out from the ImageNet[11] based on certain characteristics. By aligning with the previous work, we use the same

types of subsets: ImageNette (various objects)[20], ImageWoof (dogs)[20], ImageFruit (fruits) [4], ImageMeow (cats) [4], ImageSquawk (birds) [4], and ImageNet-[A, B, C, D, E] (based on ResNet50 performance) [5]. Each subset has 10 classes. The specific class name in each Imagenet-Subset is shown in Table 18.

C.2. Network Architecture

For the comparison of same-architecture performance, we employ a convolutional neural network ConvNet-3 as the backbone network as well as the test network. For low-resolution datasets, we employ a 3-depth convolutional neural network ConvNet-3 as the backbone network, consisting of three basic blocks and one fully connected layer. Each block includes a 3×3 convolutional layer, instance normalization [42], ReLU non-linear activation, and a 2×2 average pooling layer with a stride of 2. After the convolution blocks, a linear classifier outputs the logits. For high-resolution datasets, we employ a 5-depth convolutional neural network ConvNet-5 as the backbone network for 128×128 resolution, ConvNet-5 has five duplicate blocks, which is as the same as that in ConvNet-3. For 256×256 resolution, we employ ConvNet-6 as the backbone network.

For the comparison of cross-architecture performance, we also follow the previous work: ResNet-18 [19], VGG-11 [39], AlexNet [23], and ViT [13] from the DC-BENCH [9] resource.

C.3. Implementation details

The implementation of our proposed H-PD is based on the open-source code for GLaD [5], which is conducted on NVIDIA GeForce RTX 3090.

To ensure fairness, we utilize identical hyperparameters and optimization settings as GLaD. In our experiments, we also adopt the same suite of differentiable augmentations (originally from the DSA codebase [48]), including color, crop, cutout, flip, scale, and rotate. We use an SGD optimizer with momentum, ℓ_2 decay. The entire distillation process continues for 1200 epochs. We evaluate the performance of the synthetic dataset by training 5 randomly initialized networks on it.

To obtain the expert trajectories used in MTT, we train a backbone model from scratch on the real dataset for 15 epochs of SGD with a learning rate of 10^{-2} , a batch size of 256, and no momentum or regularization. To maintain the integration of different distillation methods, we do not use the ZCA whitening on both high-resolution datasets and low-resolution datasets different from previous work[4], which leads to a same-architecture performance drop, please note that our proposed H-PD still outperforms under the same setting. Different from GLaD which records 1000 expert trajectories for the MTT method,

Dataset	0	1	2	3	4	5	6	7	8	9
ImNet-A	Leonberg	Proboscis Monkey	Rapeseed	Three-Toed Sloth	Cliff Dwelling	Yellow Lady’s Slipper	Hamster	Gondola	Orca	Limpkin
ImNet-B	Spoonbill	Website	Lorikeet	Hyena	Earthstar	Trolleybus	Echidna	Pomeranian	Odometer	Ruddy Turnstone
ImNet-C	Freight Car	Hummingbird	Fireboat	Disk Brak	Bee Eater	Rock Beauty	Lion	European Gallinule	Cabbage Butterfly	Goldfinch
ImNet-D	Ostrich	Samoyed	Snowbird	Brabancon Griffon	Chickadee	Sorrel	Admiral	Great Gray Owl	Hornbill	Ringlet
ImNet-E	Spindle	Toucan	Black Swan	King Penguin	Potter’s Wheel	Photocopier	Screw	Tarantula	Oscilloscope	Lycaenid
ImNette	Tench	English Springer	Cassette Player	Chainsaw	Church	French Horn	Garbage Truck	Gas Pump	Golf Ball	Parachute
ImWoof	Australian Terrier	Border Terrier	Samoyed	Beagle	Shih-Tzu	English Foxhound	Rhodesian Ridgeback	Dingo	Golden Retriever	English Sheepdog
ImNet-Birds	Peacock	Flamingo	Macaw	Pelican	King Penguin	Bald Eagle	Toucan	Ostrich	Black Swan	Cockatoo
ImNet-Fruits	Pineapple	Banana	Strawberry	Orange	Lemon	Pomegranate	Fig	Bell Pepper	Cucumber	Granny Smith Apple
ImNet-Cats	Tabby Cat	Bengal Cat	Persian Cat	Siamese Cat	Egyptian Cat	Lion	Tiger	Jaguar	Snow Leopard	Lynx

Table 18. Corresponding class names in each ImageNet-Subsets. The visualizations follow the same order.

Dataset	IPC	Synthetic steps	Expert epochs	Max expert epoch	Trajectory number	Learning rate (Learning rate)	Learning rate (Teacher)	Learning rate (Latent w)	Learning rate (Latent f)	Steps per space
CIFAR-10	1	20	3	50	100	10^{-6}	10^{-2}	10^1	10^4	100
	10	20	3	50	100	10^{-6}	10^{-2}	10^1	10^4	100
ImageNet-Subset	1	20	3	15	200	10^{-6}	10^{-2}	10^1	10^4	100

Table 19. TESLA hyper-parameters

Dataset	IPC	Learning rate (Latent w)	Learning rate (Latent f)	Steps per space
CIFAR-10	1	10^{-2}	10^1	20
	10	10^{-2}	10^1	20
ImageNet-Subset	1	10^{-2}	10^1	20
	10	10^{-2}	10^1	20

Table 20. DM hyper-parameters

Dataset	IPC	inner loop	outer loop	Learning rate (Latent w)	Learning rate (Latent f)	Steps per space
CIFAR-10	1	1	1	10^{-3}	10^0	100
	10	50	10	10^{-3}	10^0	100
ImageNet-Subset	1	1	1	10^{-3}	10^0	100
	10	50	10	10^{-3}	10^0	100

Table 21. DSA hyper-parameters

we only record 200 expert trajectories and thus largely reduce the computational costs. Additionally, while GLaD performs 5k optimization epochs on the synthetic dataset using MTT as the distillation method, we only perform 1k

optimization epochs and achieve better performance both on same-architecture and cross-architecture settings, further proving the superiority of our H-PD. The detailed hyperparameters are shown in Table 20, Table 21 and Table 19.

D. More Visualizations

We provide additional visualizations of synthetic datasets generated by H-PD using diverse distillation methods, as shown in Figure 10, Figure 11, and Figure 12.

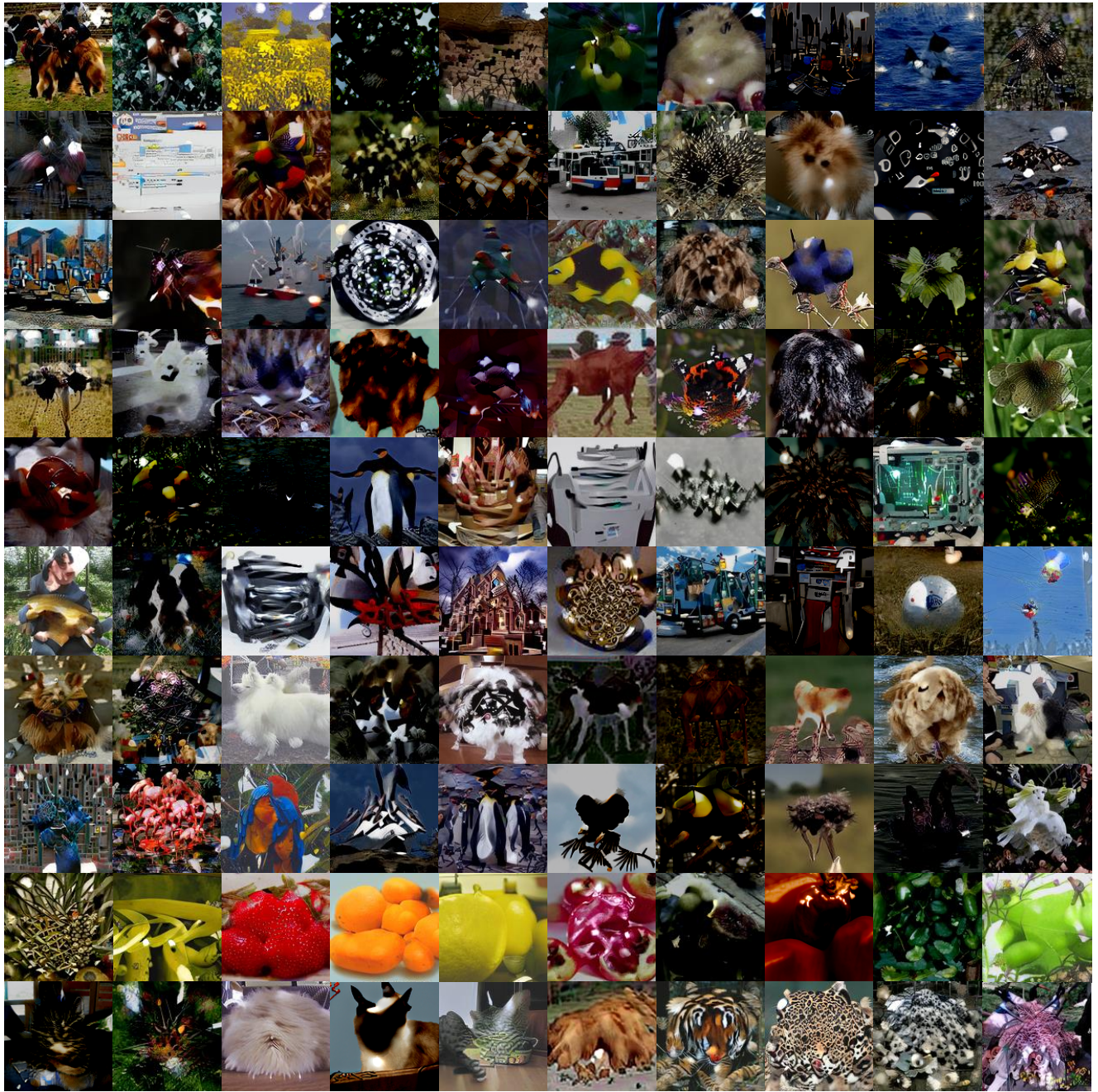


Figure 10. More visualization of the synthetic datasets using TESLA.

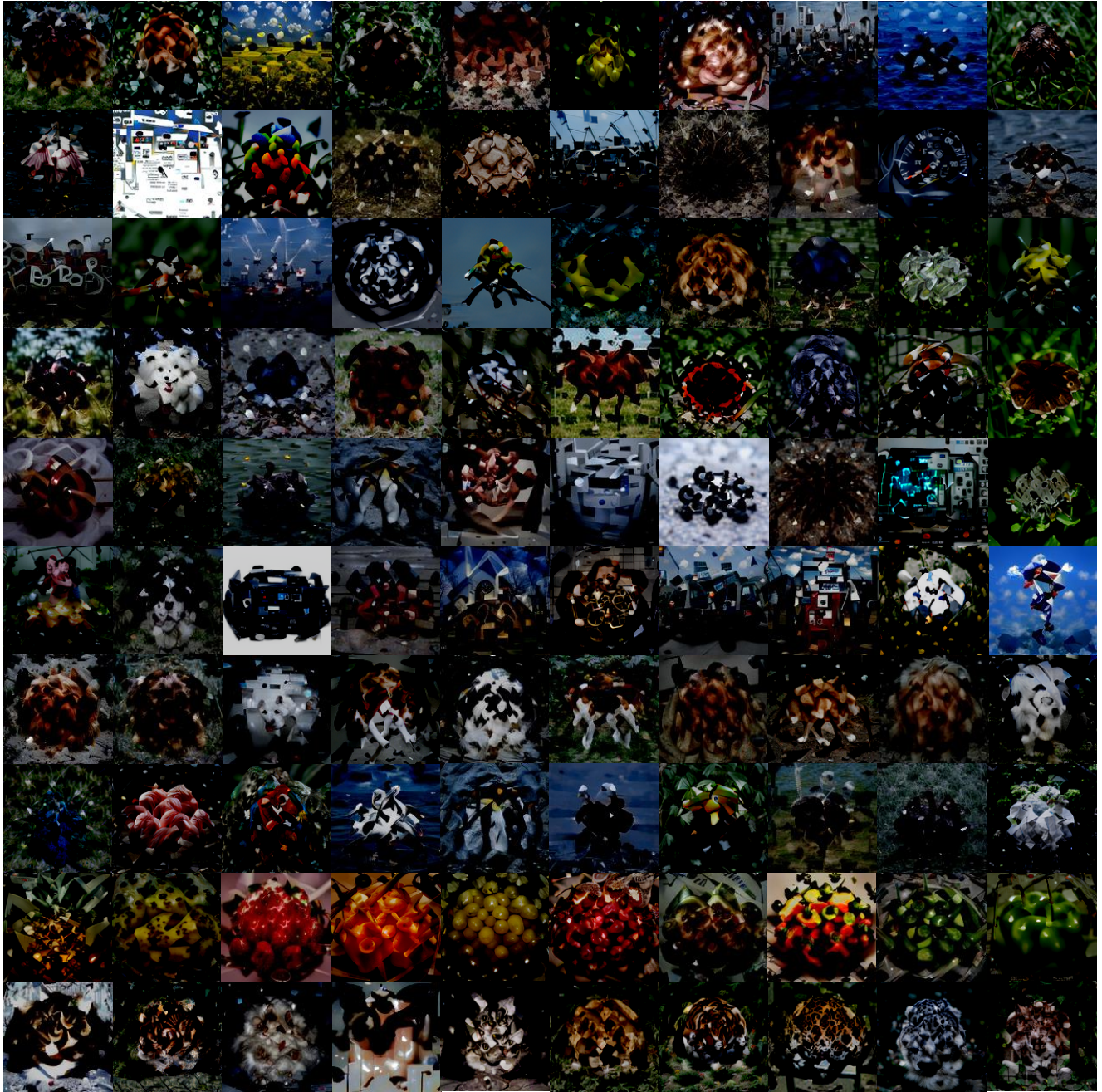


Figure 11. More visualization of the synthetic datasets using DSA.

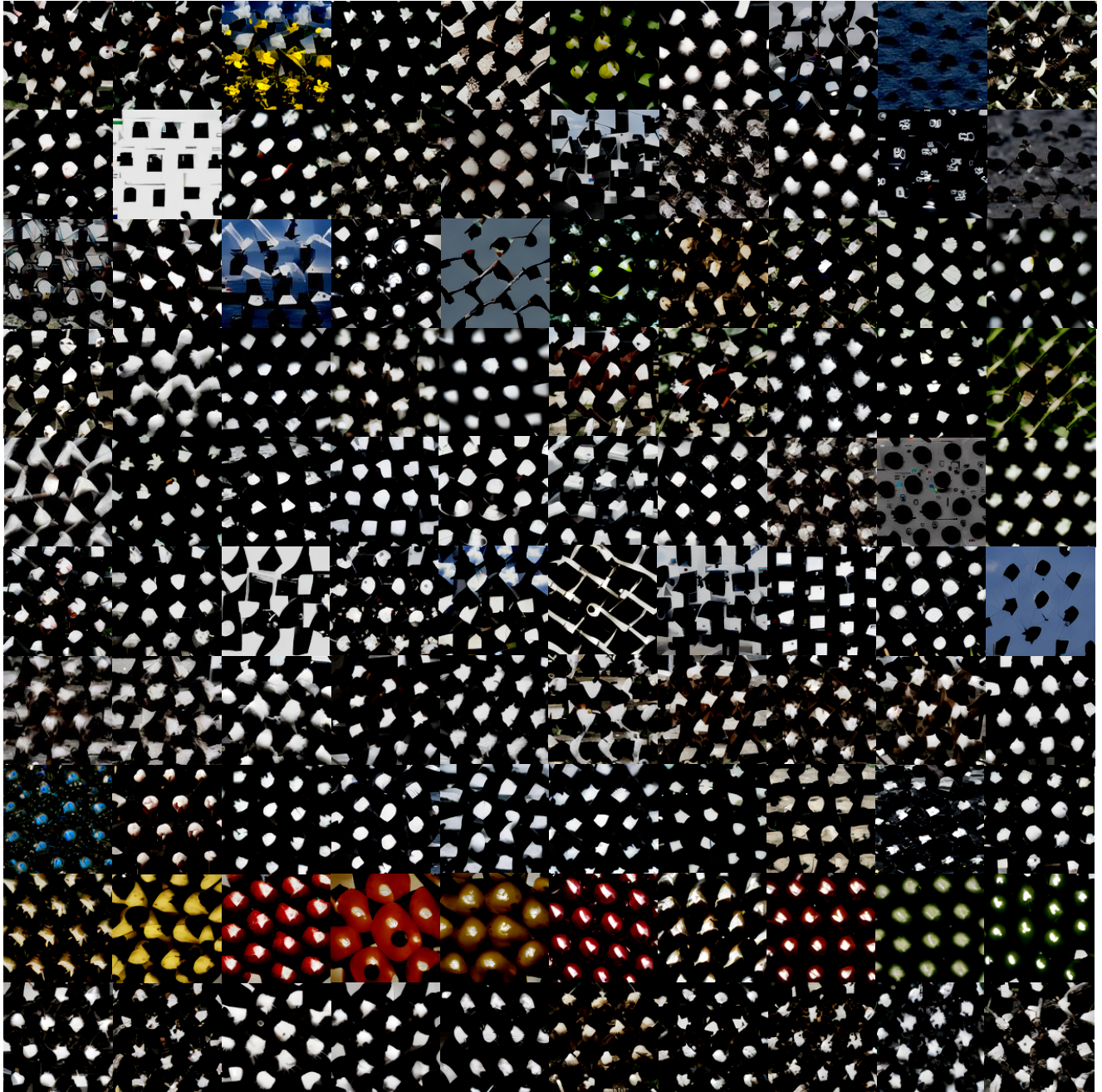


Figure 12. More visualization of the synthetic datasets using DM.